

Coregulation of extracellular vesicle production and fluconazole susceptibility in *Cryptococcus neoformans*

Juliana RIZZO^{1,2#§}, Adèle TROTTIER^{1#}, Frédérique MOYRAND^{1#}, Jean-Yves COPPEE^{1#}, Corinne MAUFRAIS^{1,3#}, Ana Claudia G. ZIMBRES^{2#}, Thi Tuong Vi DANG^{1#}, Alexandre ALANIO^{8,9}, Marie Desnos-OLLIVIER⁸, Isabelle MOUYNA^{1#}, Gérard PÉHAU-ARNAUDET⁴, Pierre-Henri COMMERE⁵, Sophie NOVAULT⁵, Juliana V. ENE⁶, Leonardo NIMRICHTER^{2#}, Marcio L. RODRIGUES^{2,7#} and Guilhem JANBON^{1,*#}

¹ Institut Pasteur, Université Paris Cité, Unité Biologie des ARN des Pathogènes Fongiques, F-75015 Paris, France

² Instituto de Microbiologia Paulo de Góes (IMPG), Universidade Federal do Rio de Janeiro, Rio de Janeiro, Brazil

³ Institut Pasteur, Université Paris Cité, USR 3756 IP CNRS, HUB Bioinformatique et Biostatistique, F-75015, Paris, France

⁴ Institut Pasteur, Université Paris Cité, Plateforme de Bio-Imagerie Ultrastructurale, F-75015 Paris, France

⁵ Institut Pasteur, Université Paris Cité, Cytometry and Biomarkers, F-75015, Paris, France

⁶ Institut Pasteur, Université Paris Cité, Fungal Heterogeneity Group, F-75015 Paris, France

⁷ Instituto Carlos Chagas, Fundação Oswaldo Cruz (FIOCRUZ), Curitiba, Brazil

⁸ Institut Pasteur, Université Paris Cité, Centre National de Référence Mycoses Invasives et Antifongiques, Groupe de recherche Mycologie Translationnelle, Département de Mycologie, F-75015 Paris, France

⁹ Laboratoire de parasitologie-mycologie, AP-HP, Hôpital Saint-Louis, F-75010 Paris, France

* Corresponding author: janbon@pasteur.fr

[#] Members of the data sharing transparency group on fungal extracellular vesicles

§ Current affiliation: Instituto de Biofísica Carlos Chagas Filho (IBCCF), Universidade Federal do Rio de Janeiro, Rio de Janeiro, Brazil

ABSTRACT (150/150 words)

Resistance to fluconazole (FLC), the most widely used antifungal drug, is typically achieved by altering the azole drug target and/or drug efflux pumps. Recent reports have suggested a link between vesicular trafficking and antifungal resistance. Here, we identified novel *Cryptococcus neoformans* regulators of extracellular vesicle (EV) biogenesis that impact FLC resistance. In particular, the transcription factor Hap2 does not affect the expression of the drug target or efflux pumps, yet it impacts the cellular sterol profile. Subinhibitory FLC concentrations also downregulate EV production. Moreover, *in vitro* spontaneous FLC-resistant colonies showed altered EV production, and the acquisition of FLC resistance was associated with decreased EV production in clinical isolates. Finally, the reversion of FLC resistance was associated with increased EV production. These data suggest a model in which fungal cells can regulate EV production in place of regulating the drug target gene expression as a first line of defense against antifungal assault in this fungal pathogen.

IMPORTANCE

Extracellular vesicles (EVs) are membrane-enveloped particles that are released by cells into the extracellular space. Fungal EVs can mediate community interactions and biofilm formation but their functions remain poorly understood. Here, we report the identification of the first regulators of EV production in the major fungal pathogen *Cryptococcus neoformans*. Surprisingly, we uncover a novel role of EVs in modulating antifungal drug resistance. Disruption of EV production was associated with altered lipid composition and changes in fluconazole susceptibility. Spontaneous azole-resistant mutants were deficient in EV production, while loss of resistance restored initial EV production levels. These findings were recapitulated in *C. neoformans* clinical isolates, indicating that azole resistance and EV production are coregulated in diverse strains. Our study reveals a new mechanism of drug resistance in which cells adapt to azole stress by modulating EV production.

KEYWORDS

53 *Cryptococcus neoformans*, extracellular vesicles, antimicrobial resistance, fluconazole,
54 transcription factor.

55

56 1) INTRODUCTION

57

58 Fungal diseases have been consistently neglected despite their increasing impact on human
59 health. These eukaryotic pathogens infect ~1.5 billion people worldwide and lead to ~1.5 million
60 deaths annually^{1,2}. Over 90% of reported fungal-associated deaths are caused by species from four
61 genera *Aspergillus*, *Cryptococcus*, *Candida*, or *Pneumocystis*³. The species *Cryptococcus neoformans*,
62 *Candida albicans*, *Candida auris*, and *Aspergillus fumigatus* form the critical priority group within the
63 fungal pathogens list published by the World Health Organization (WHO) in 2022^{4,5}. Fungal infections
64 are generally difficult to treat, and mortality rates remain high despite available antifungal
65 treatments⁶. The arsenal of antifungal molecules is based on four main classes: polyenes (e.g.,
66 amphotericin B), azoles (e.g., fluconazole (FLC)), echinocandins (e.g., caspofungin), and flucytosine (a
67 pyrimidine analog)⁷. Due to their bioavailability, low toxicity, and wide spectrum of action, azoles are
68 the most widely used antifungals. Azoles are fungistatic drugs that inhibit the cytochrome P450-
69 dependent enzyme 14- α demethylase encoded by *ERG11* in fungi, thus interrupting the synthesis of
70 ergosterol⁶. In azole-treated cells, an accumulation of toxic intermediate sterols is observed,
71 increasing membrane permeability and inhibiting fungal growth⁸. Prolonged use of FLC has the
72 potential to select FLC-resistant strains⁸. Azole resistance has been associated with mutations in the
73 *ERG11* sequence, thus limiting azole binding⁸, or in transcription factors (TF) like *TAC1* or *UPC1*
74 regulating the expression of *ERG11* and/or drug efflux pumps^{9,10}. Heteroresistance has also been
75 described in *C. neoformans*, and was associated with the unstable duplication of chromosome 1,
76 resulting in the potential overexpression of *ERG11* and the efflux pump encoding gene *AFR1*^{11,12}.

77 Extracellular vesicles (EVs) are cell-derived membrane particles released to the extracellular
78 space known to be produced in all domains of life. In fungi, they have been isolated from at least
79 fifteen different genera¹³. *Cryptococcus* EVs display extensive diversity in size, shape, and structure¹⁴
80 and most EVs appear decorated by fibrillary material composed of mannoproteins, and are covered
81 by capsule polysaccharide-like material¹⁴. EVs contain lipids (including ergosterol), polysaccharides,
82 small molecules, pigments, and RNAs, although our understanding of the exact composition and
83 function of these cargo molecules remains limited¹².

84 The involvement of vesicular trafficking in fungal FLC resistance has been previously
85 suggested. For instance, turbinmicin, a molecule with a broad spectrum antifungal activity, targets
86 Sec14p in the post-Golgi vesicular trafficking pathway and synergizes with FLC against *C. albicans*
87 biofilm formation¹⁵. Sortin2 inhibition of vesicular transport potentiates azoles in *C. albicans* and *C.*
88 *glabrata*¹⁶. Studies in *C. neoformans* and *S. cerevisiae* have implicated Golgi trafficking and vesicle

89 formation as potential avenues of azole potentiation¹⁷⁻¹⁹. Recent studies also suggested that EVs
90 released by fungi could play a role in antifungal resistance²⁰⁻²³. For instance, *C. albicans* EVs confer FLC
91 resistance to biofilms and ESCRT (endosomal sorting complexes required for transport) mutants
92 defective in EVs production show altered biofilm FLC resistance²⁰. EVs from *C. auris* drug-resistant
93 strain induced amphotericin-B resistance to a susceptible strain²¹, but the mechanisms underlying this
94 process remain largely unknown. Other examples of EVs associated with drug resistance come from
95 the study of *Leishmania* parasites²⁴, where EVs mediate the delivery of drug-resistance genes, leading
96 to the emergence of resistant subpopulations²⁴.

97 Despite these intriguing connections, the study of fungal EV biosynthesis in the context of
98 antifungal resistance has been constrained by our limited understanding of EV biosynthesis. Genetic
99 analyses of EV production and regulation have been hampered by the long and cumbersome protocols
100 necessary to isolate and study these particles. Only a handful of mutations associated with defects in
101 EV production have been reported so far, as recently reviewed¹³.

102 To narrow this knowledge gap, we screened a *C. neoformans* TF mutant library²⁵ and identified
103 the first regulators of EV biogenesis in fungi. We present data revealing a phenotypic association
104 between drug resistance and regulation of EV biogenesis in these mutant strains but also in
105 spontaneous FLC-resistant mutants isolated *in vitro*, as well as in clinical isolates. Moreover, we
106 demonstrate that EV-defective mutants show altered lipid content. Finally, we show that sub-
107 inhibitory concentrations of FLC regulate EV production. Taken together, our study points to a new
108 mechanism of drug resistance in which cells adapt to FLC stress by modulating EV production. Our
109 results uncover key regulators of EV biogenesis in *C. neoformans*, as well as a novel link with antifungal
110 drug resistance.

111

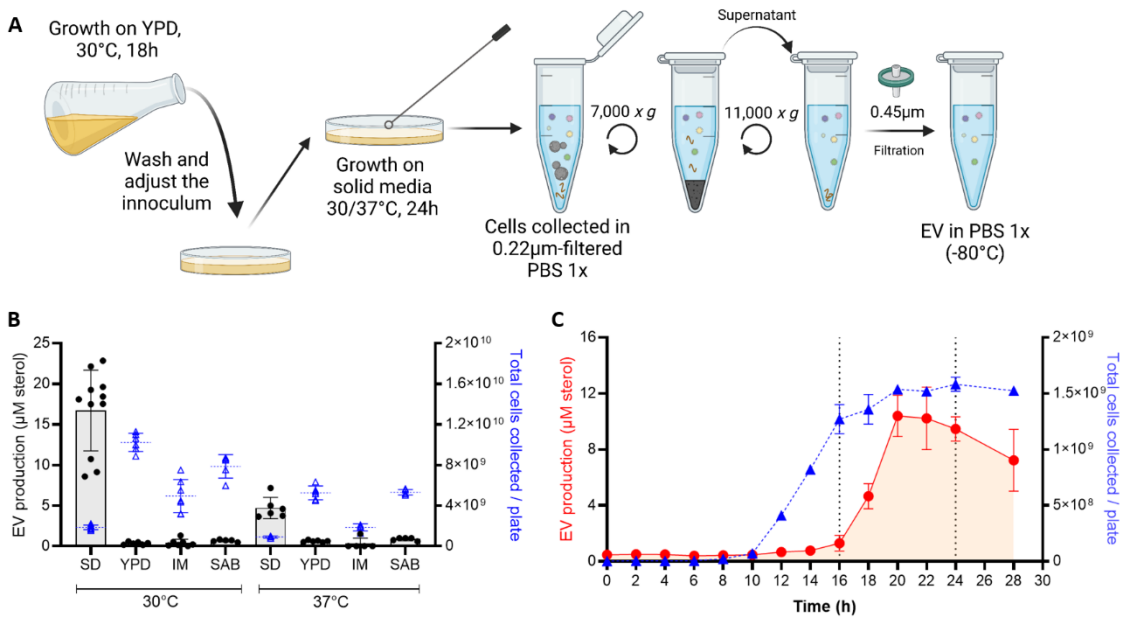
112 2) RESULTS

113

114 a) EV production is regulated by growth conditions and growth phase in *C. neoformans*.

115 To test whether EV production varies across different media, growth stages, and
116 temperatures, we optimized a new EV isolation protocol, in which the ultracentrifugation step was
117 bypassed (**Fig 1A**). We used this protocol to demonstrate that EV production, as measured by the
118 amount of total sterol in cellular supernatants, was highest when cells were grown in synthetic
119 dextrose (SD) medium at 30°C compared to the other conditions tested (**Fig 1B**). By exploring the
120 dynamics of EV production during the growth on SD agar plates at 30°C, we noticed that cells release
121 EVs during a limited time window (16 to 24 h) corresponding to the transition between the exponential
122 to stationary growth phase (**Fig 1C**).

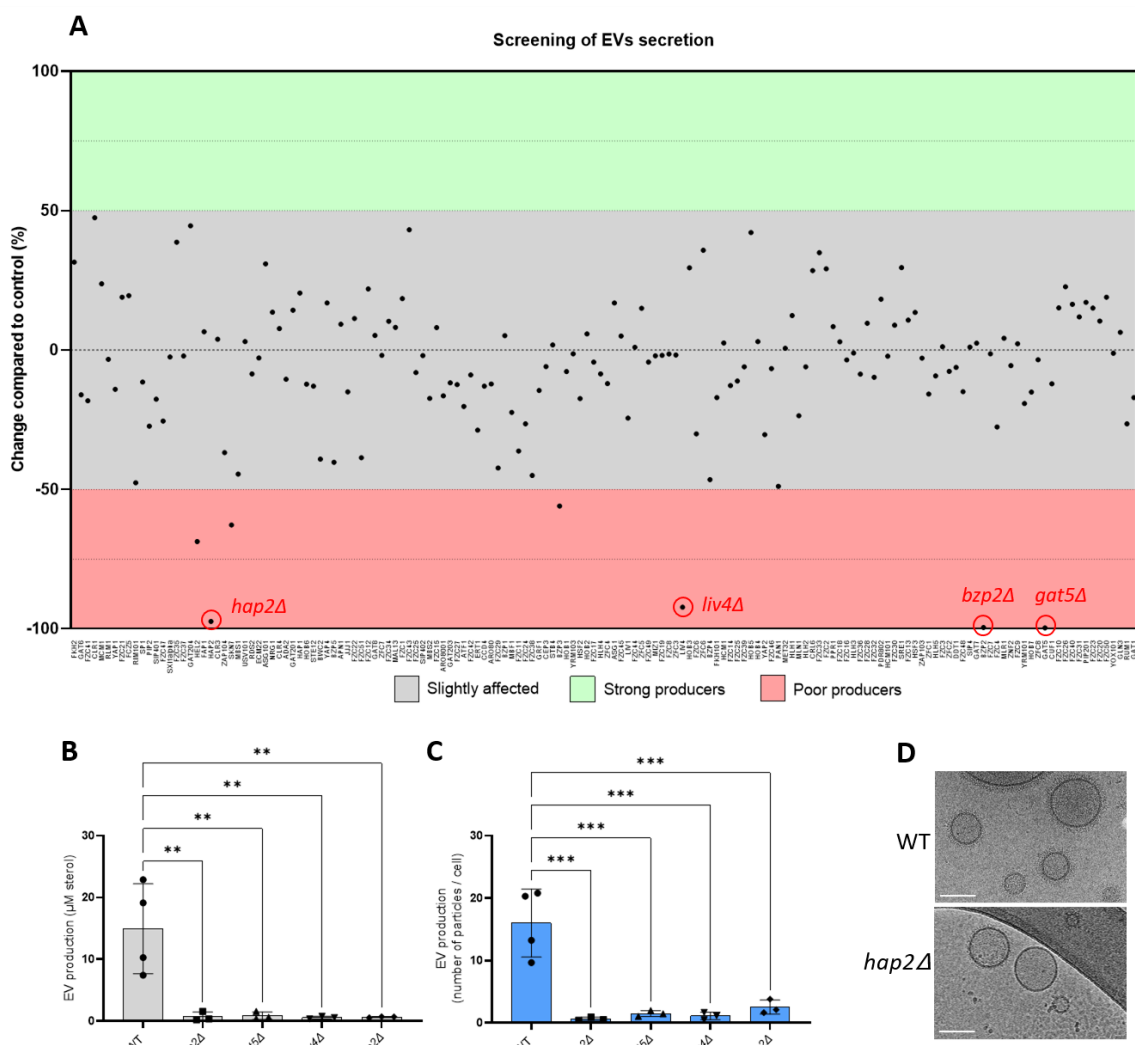
123



124
125 **Figure 1: EV production is regulated by growth conditions and growth phase.** Schematic representation of the optimized
126 quick protocol used to obtain EVs from cells grown on solid medium (A). EV production from cells grown on different media:
127 synthetic dextrose (SD), yeast extract-peptone-dextrose (YPD), capsule induction media (IM), and Sabouraud (SAB) at 30°C
128 and 37°C, sterol concentration values are expressed per 10⁹ cells for each condition (B). EV production on SD medium at 30°C
129 during the growth curve was analysed by the amount of total sterol in cellular supernatants when EVs are isolated using the
130 quick protocol, values are expressed per plate of culture during each timepoint (C). Experiments were done with three or
131 more biological replicates. Error bars show means ± SD. Schematic representation created in BioRender.

132
133
134
135 **b) Identification of regulators of EV production in *C. neoformans*.**

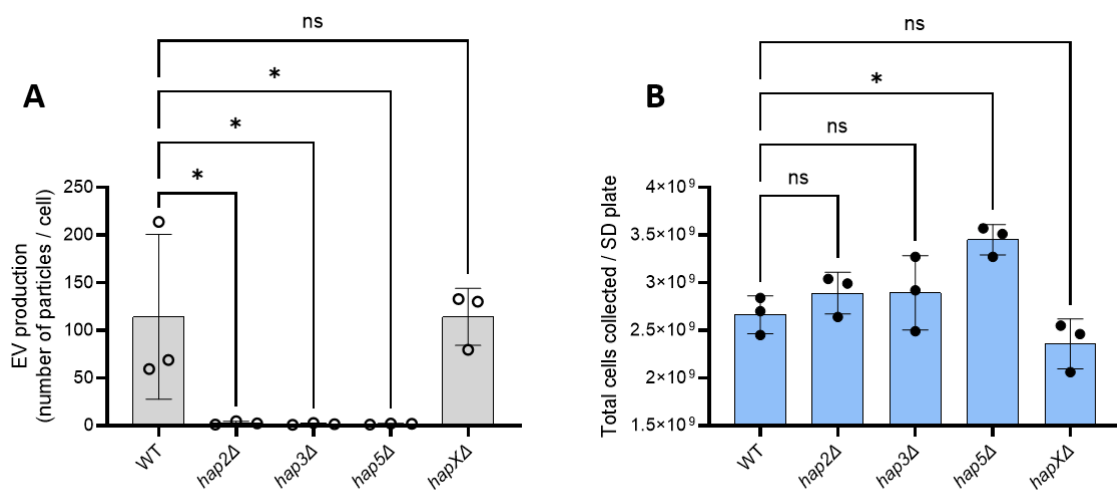
136 The tight regulation between EV production and growth suggested that specific TFs might
137 regulate their biosynthesis. Thus, to identify potential regulators of EV biogenesis, we screened a
138 collection of 155 TF mutants²⁵ using the EV purification optimized protocol adjusted to 96-well plates
139 (**Fig 2A**). We identified four mutants strongly altered in EV production. These strains produced <10%
140 of the WT EV levels as evaluated by the total amount of sterols in EV samples. The EV-deficient strains
141 lacked TFs *BZP2* (CNAG_04263), *GAT5* (CNAG_05153), *LIV4* (CNAG_06283) and *HAP2* (CNAG_07435).
142 These results were confirmed when samples were prepared using the conventional
143 ultracentrifugation protocol¹⁴, measuring the total amount of sterols (**Fig 2B**), and evaluating the
144 number of particles by nanoparticle flow cytometry (nanoFCM) analysis (**Fig 2C**). It is important to
145 note that despite an impressive decrease in EV levels, these TF mutants were not completely impaired
146 in EV production, as the high sensitivity of the nanoFCM analysis used detected EV-like particles in
147 each of the EV samples obtained from the mutants. Moreover, using a large number of culture plates,
148 we obtained enough *hap2Δ*-derived EVs to be observed by Cryo-EM. Image analysis revealed a similar
149 structure of *hap2Δ* EVs as previously observed for WT EVs¹⁴ (**Fig 2D**).



151 **Figure 2: Identification of the transcription factors regulating EV production in *C. neoformans*.** The screening of a 155
 152 transcription factor (TF) mutant collection identified four major EV production regulators: *HAP2*, *LIV4*, *BZP2*, and *GAT5* (A).
 153 Confirmation of the EV phenotype using independent knockout strains generated in the KN99 α background by measuring
 154 the amount of total sterol contained in EV samples. Sterol concentration values are expressed per 10^9 cells for each
 155 condition (B) and single particle counting using nanoFCM (C). Cryo-EM analysis of EVs obtained from WT and *hap2* Δ strains
 156 (D), scale bar = 100 nm. Experiments were performed in at least three biological replicates. Error bars show means \pm SD.
 157

158 *Bzp2p* and *Gat5p* belong to a conserved zinc finger family containing TFs known as GATA-
 159 factors, regulating radiation sensitivity and nitrogen catabolite repression (NCR) when preferred
 160 nitrogen sources are absent or limiting²⁶. *Liv4p* is a conserved MYB-like DNA-binding domain TF
 161 regulating growth and virulence in *C. neoformans*²⁷. *Hap2p* is a subunit of the evolutionary conserved
 162 CCAAT-binding heme activator protein (HAP) complex, a heterotrimeric complex composed of
 163 *Hap2/3/5* and the transcriptional activation subunit, *HapX*²⁸. As expected, the *hap3* Δ and *hap5* Δ
 164 mutants were also drastically impaired for EV production. In contrast, the *hapX* Δ mutant strain
 165 produced the same quantity of EVs as the WT strain (Fig 3A), suggesting that the *Hap2/3/5* complex
 166 controls EV production in an *HapX*-independent manner in *C. neoformans*. Notably, whereas *bzp2* Δ ,

167 *liv4Δ*, and *gat5Δ* mutant strains displayed reduced growth (**Fig S1**), none of the *hap* mutant strains
168 showed growth deficiency under the conditions used to obtain EVs (**Fig 3B**).

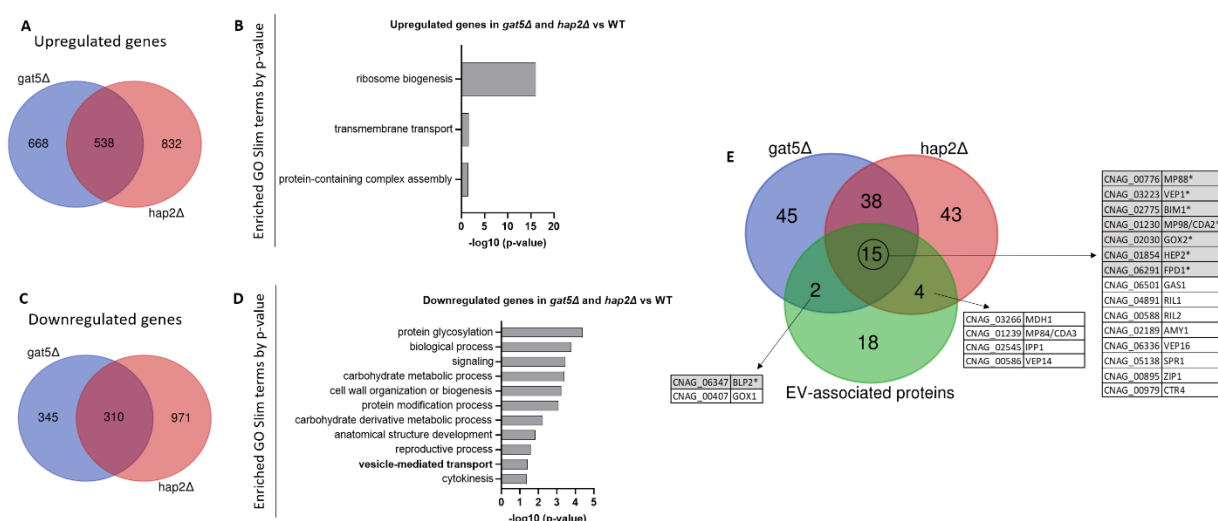


169
170 **Figure 3:** The *HAP2/3/5* complex is involved in EV secretion. Quantification of single EV particles released by WT and HAP
171 complex mutants using nanoFCM (A). Growth analysis by counting the total number of cells obtained from SD plates (B). The
172 experiments were carried out in biological triplicates. Error bars show means ± SD.

173
174 **c) Transcriptional analysis of EV-defective mutants**

175 To decipher the link between the expression of these TF and the EV production phenotype of their
176 corresponding mutants, we performed the RNA-seq analysis of the *hap2Δ*, *gat5Δ* and WT strains
177 grown for 18 h on SD plates at 30°C, a condition which corresponds to the maximum EV production
178 (see **Fig 1C**). Differential expression gene analysis identified 538 genes commonly upregulated in both
179 *hap2Δ* and *gat5Δ* strains (**Fig 4A**) (**Supplementary Table S1**). Gene ontology (GO) analysis using the
180 FungiDB database (<https://fungidb.org/fungidb/app>), revealed that genes associated with ribosome
181 biogenesis, transmembrane transport, and protein-containing complex assembly were enriched in this
182 set (**Fig 4B**). This suggests that the downregulation of the translation machinery expected to occur
183 during the transition from the exponential phase to the stationary phase²⁹ is impaired in both mutant
184 strains. On the other hand, 310 genes were downregulated in both mutant strains (**Fig 4C**)
185 (**Supplementary Table S1**). GO analysis revealed genes coding for proteins implicated in protein
186 glycosylation, signaling, carbohydrate metabolic processes, cell wall organization and biogenesis,
187 protein modification process, carbohydrate metabolism, reproductive processes, vesicle-mediated
188 transport, as well as cytokinesis, as being enriched in this set (**Fig 4D**). Interestingly, *GAT5* expression
189 is strongly downregulated (10-fold) in the *hap2Δ* mutant, suggesting that Hap2 might act upstream of
190 *GAT5* in regulating EV production. In contrast, neither *BZP2* nor *LIV4* appeared regulated by *HAP2*
191 and/or *GAT5*, suggesting an independent regulation pathway. We then considered the top-100 most
192 expressed genes in WT within the lists of *gat5Δ*, or *hap2Δ* downregulated genes reasoning that the

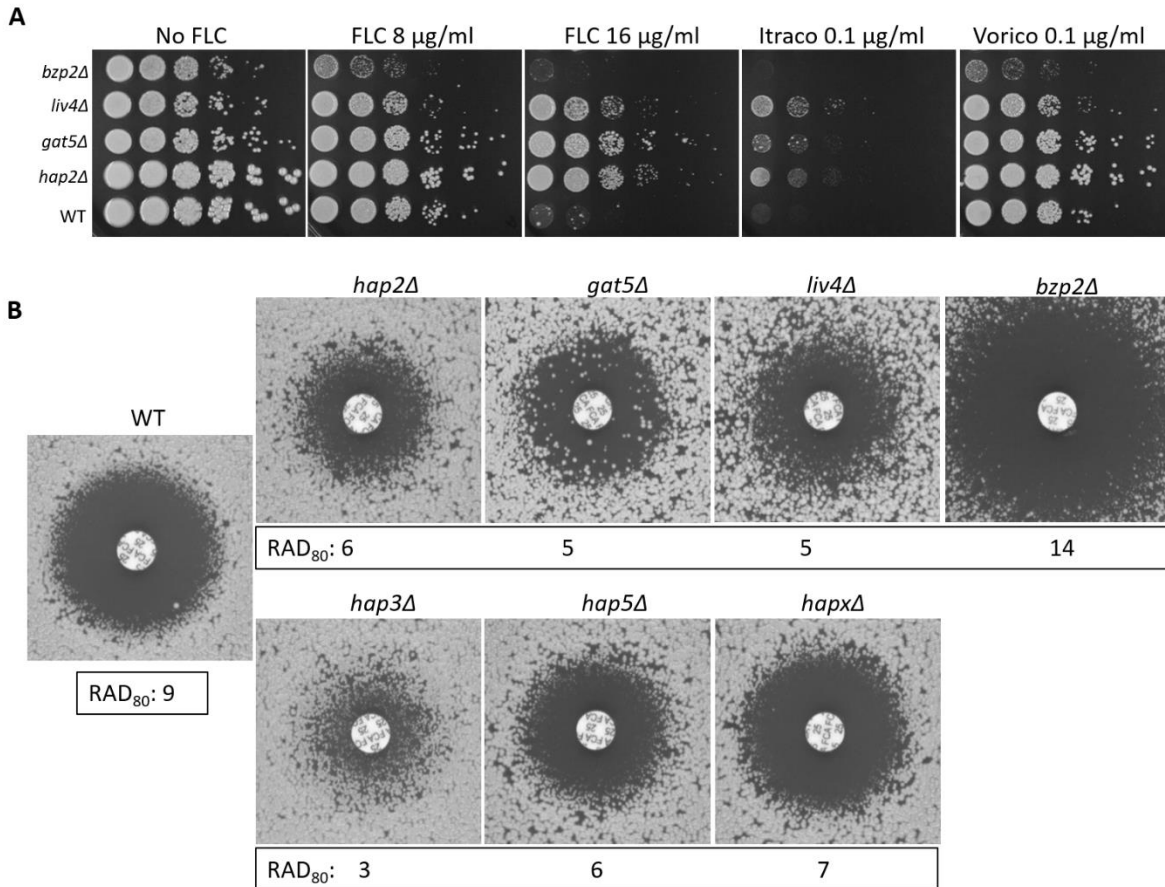
193 impact of a gene downregulation associated with a mutation would have a phenotypic consequence
 194 if this gene is strongly expressed in the WT strain. Interestingly, 21 of the 39 previously identified *C.*
 195 *neoformans* enriched EV-protein encoding genes¹⁴ were regulated by either *GAT5* or *HAP2* (Fig. 4E).
 196 In addition, the 15 genes coding for EV proteins regulated by both TFs included seven proteins
 197 belonging to the top ten most abundant EV-associated proteins in *C. neoformans*. Thus, *HAP2* and
 198 *GAT5* regulate the expression of many EV-associated protein components, confirming their function
 199 as major regulators of EV production in *C. neoformans*.



200
 201 **Figure 4:** Transcriptomic analysis of the EV-deficient mutants *hap2 Δ* and *gat5 Δ* grown in EV-producing conditions. Venn
 202 diagram revealing the number of upregulated genes in both mutants (A). Analysis of the GO SLIM categories enriched in the
 203 the group of genes upregulated in both mutants (B). Venn diagram revealing the number of the downregulated genes in both
 204 mutants (C). GO SLIM categories enriched in the group of downregulated genes in both mutants (D). Venn diagram revealing
 205 the overlap between genes downregulated in *gat5 Δ* and *hap2 Δ* , and the ones coding for the EV-enriched proteins of *C.*
 206 *neoformans*, previously identified by proteomics (E). The genes highlighted in grey with an asterisk encode proteins among
 207 the ten most abundant proteins in *C. neoformans* EVs.
 208
 209

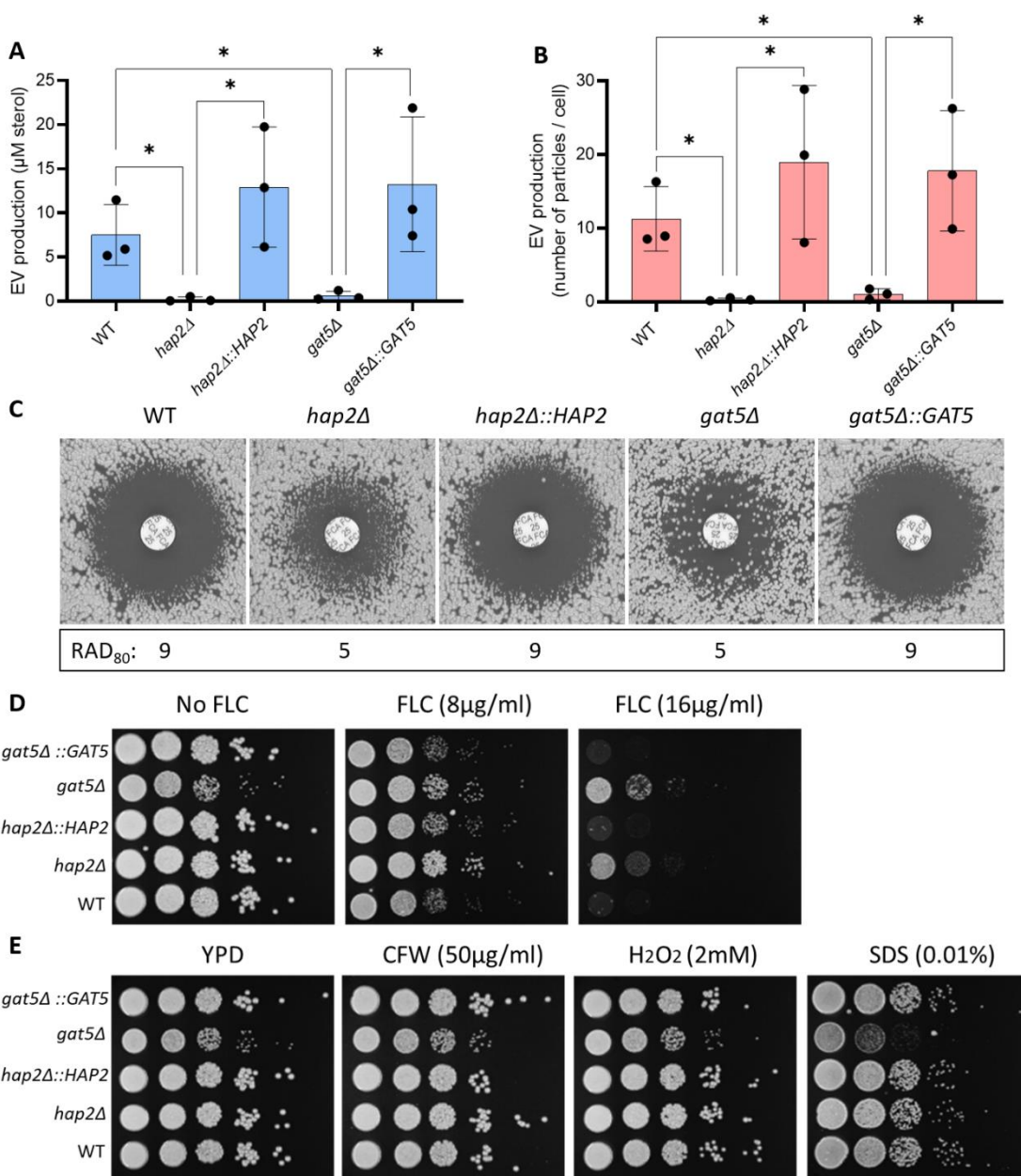
210 **d) EV production regulator mutant strains are altered in azole susceptibility**

211 Strikingly, all four newly identified EV production mutant strains have been reported to have
 212 altered FLC sensitivity in the systematic phenotypic analysis of the TF mutants published by the Bahn's
 213 laboratory²⁵. Indeed, we confirmed that *hap2 Δ* , *gat5 Δ* , and *liv4 Δ* were less susceptible to FLC, while
 214 *bzp2 Δ* was more susceptible compared to the WT strain (Fig 5A-B). Similar phenotypes were observed
 215 with Itraconazole and Voriconazole (Fig 5A). We also tested the FLC susceptibility of the *hap* mutants
 216 and noticed that those impaired in EV production (i.e., *hap2 Δ* , *hap3 Δ* , and *hap5 Δ*) were also more
 217 resistant to FLC. In contrast, the *hapX Δ* mutant strain, which showed no alteration in EV production
 218 (Fig3A), only displayed slight differences in FLC sensitivity (Fig 5B).



219
220 **Figure 5:** Transcription factors regulating EV release are associated with altered azole susceptibility. Spot assay for
221 Fluconazole (FLC), Itraconazole (Itraco) and Voriconazole (Vorico) susceptibility (A) and FLC diffusion disk diffusion assay (25
222 μ g/disk) for the four EV-defective TF mutants identified in the screening (*hap2Δ*, *gat5Δ*, *liv4Δ* and *bzp2Δ*), and for all the
223 members of HAP complex inlcuing *hap3Δ* , *hap5Δ* and *hapXΔ*, grown for 72h (B). Average RAD₈₀ values obtained from
224 diskImageR analyses are provided. The results are illustrative of three biological replicates.

225
226 Accordingly, reconstruction of the *gat5Δ* and *hap2Δ* mutant strains restored both phenotypes to
227 WT levels (Fig 6A-D). We also evaluated the sensitivity of these strains to agents that disturb the cell
228 wall and plasma membrane, such as Calcofluor white - CFW, hydrogen peroxide - H₂O₂, and sodium
229 dodecyl sulfate – SDS, and observed that only *gat5Δ* was more susceptible to the presence of SDS (Fig
230 6E). Overall the analysis of TF mutant strains suggested that EV production and FLC susceptibility are
231 coregulated.

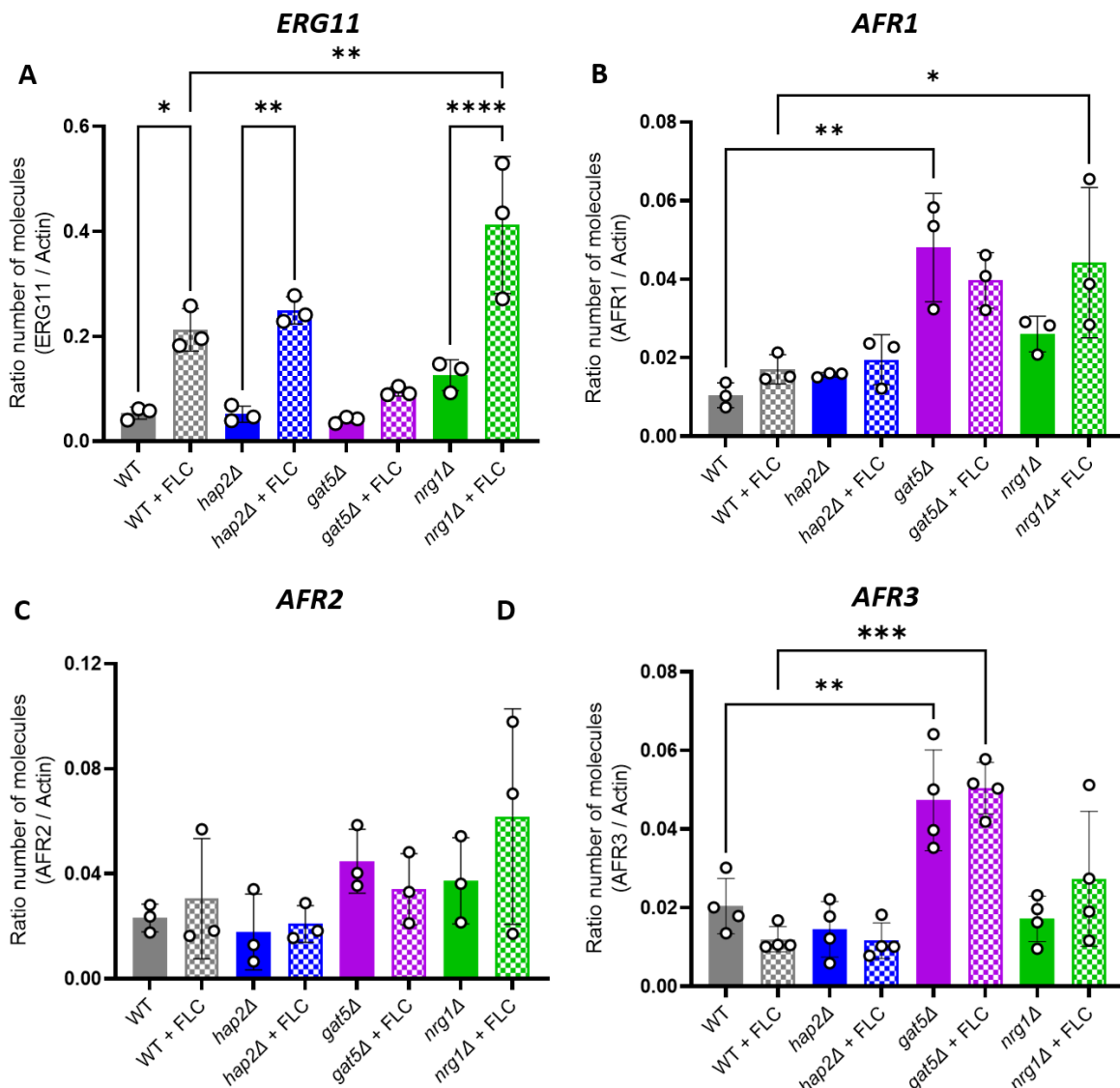


232
233 **Figure 6:** Complementation of the *hap2Δ* and *gat5Δ* mutant strains restores the phenotypes of EV production and FLC
234 susceptibility. Total sterol contents in EVs produced by WT, mutants, and complemented cells. Sterol concentration values
235 are expressed per 10^9 cells for each condition (A). Quantification of EV particles using nanoFCM in WT, mutants and
236 complemented strains (B). FLC susceptibility by disk diffusion assay (25 μ g/disk) and RAD₈₀ values obtained by diskImageR
237 (C). FLC susceptibility analysis by spot assay (D). Growth analysis in the presence of cell wall and plasma membrane disturbing
238 agents (Calcofluor White - CFW, Hydrogen Peroxide - H₂O₂, and Sodium Dodecyl Sulfate – SDS (E). The experiments were
239 carried out in biological triplicates. Error bars show means \pm SD.

240
241 **e) *hap2Δ* FLC resistance is not associated with *ERG11* or *AFR* genes over expression**
242 In *C. neoformans*, FLC resistance has been associated with either mutation of *ERG11*
243 (CNAG_00040) and/or the overexpression of efflux pumps genes such as *AFR1* (CNAG_00730), *AFR2*
244 (CNAG_00869) and *AFR3* (CNAG_06909)³⁰. Interestingly, differential gene expression analysis of
245 *gat5Δ*, *hap2Δ*, and WT cells grown under conditions of EV production revealed that neither mutation
246 was associated with an increased expression of any of these resistance genes. We then used RT-qPCR

247 assays to evaluate the expression levels of *ERG11* and the *AFR* genes in the presence or absence of
248 FLC in these genetic backgrounds. As an additional control, we also included a strain lacking *NRG1*
249 (CNAG_05222), which was shown to be FLC resistant²⁵ but was found here to produce WT EV levels
250 (**Fig S2**). In the absence of FLC, we did not observe changes in *ERG11* expression associated with either
251 *HAP2* or *GAT5* deletion (**Fig 7A**). In the presence of the drug, the expression of *ERG11* in the *hap2Δ*
252 mutant strain was similar to the WT, whereas in *gat5Δ*, we observed a two-fold reduction expression.
253 In contrast, in the *nrg1Δ* mutant strain, we observed a two-fold overexpression of *ERG11* as compared
254 to the WT strain. Thus, the FLC resistance phenotype in *hap2Δ* and *gat5Δ* mutants cannot be explained
255 by an alteration in *ERG11* expression levels (**Fig 7A**).

256 In contrast to *ERG11*, the presence of FLC did not impact the expression of *AFR* genes in any
257 of these strains (**Fig 7B–C–D**). However, *AFR1* and *AFR3* but not *AFR2* were upregulated in the *gat5Δ*
258 mutant (both with and without FLC), suggesting that these two efflux pumps could play a role in
259 driving FLC resistance in this strain (**Fig 7B–C–D**). A similar result was obtained with the *nrg1Δ*
260 mutant, although to a lesser extent for *AFR3*. Interestingly, in the *hap2Δ* strain, the expression of the
261 *AFR* genes was not altered, suggesting that additional mechanisms are driving FLC resistance in these
262 cells.



263

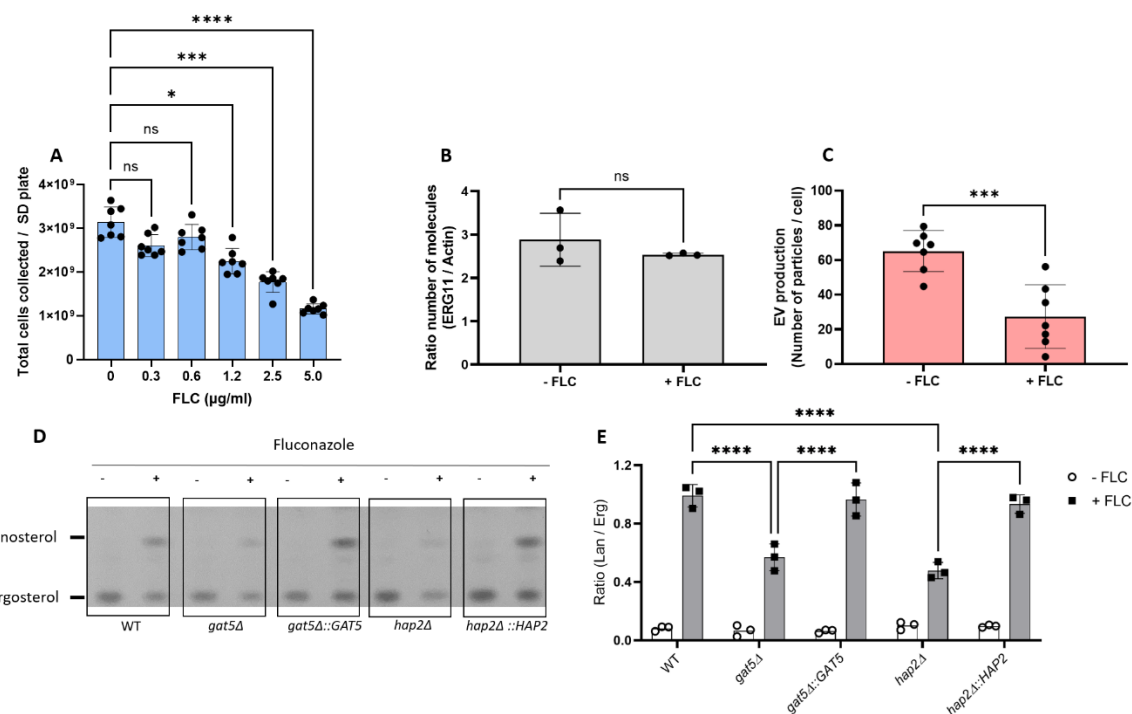
264 **Figure 7:** Gene expression analysis of known FLC resistance regulators in *C. neoformans*. *ERG11* (A), *AFR1* (B), *AFR2* (C), and
265 *AFR3* (D) gene expression profile as generated by RT-qPCR. The experiments were carried out in at least biological triplicates.
266 Error bars show means ± SD.

267

268 **f) FLC regulates EV production and cellular lipid profile**

269 The analysis of the EV regulators suggests that changes in EV production impact FLC resistance.
270 We then studied the converse relationship and tested whether FLC could modulate EV production in
271 *C. neoformans*. We first tested the growth of WT cells on SD containing FLC at different concentrations
272 (0.3, 0.6, 1.25, 2.5, and 5 µg/mL) identifying 0.6 µg/mL as the highest FLC concentration, which was
273 not affecting cellular growth (Fig 8A). At this concentration, the expression of *ERG11* was not altered
274 (Fig 8B). However, EV production was reduced by 2.4-fold (Fig 8C), suggesting that FLC regulates EV
275 production levels.

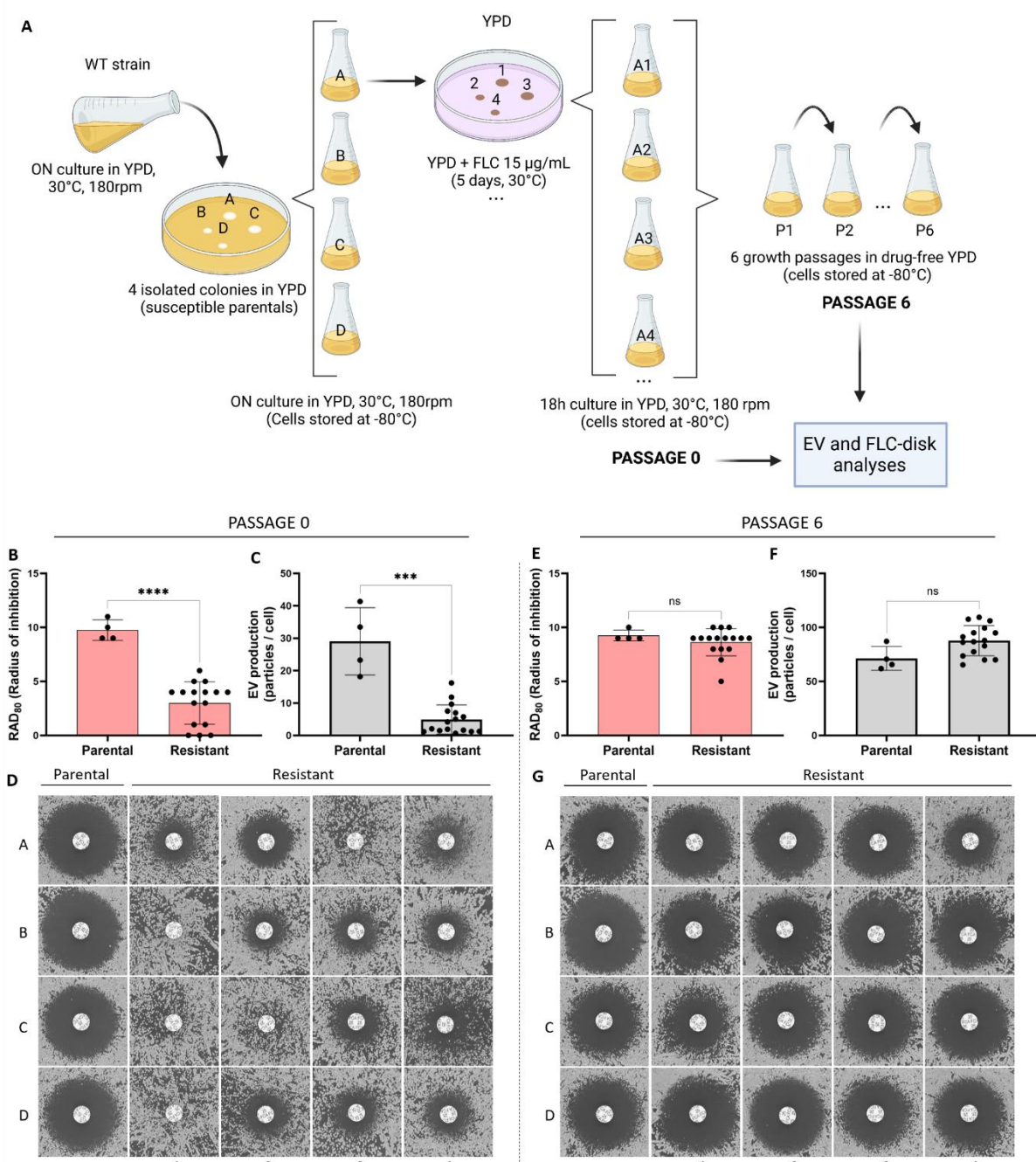
276 FLC is an inhibitor of the Erg11 lanosterol 14-demethylase, which transforms lanosterol in 4,4-
277 dimethyl-cholesta-8,14,24-trienol in the fungal ergosterol biosynthetic pathway³¹. We thus compared
278 the cellular lipid profile in WT and EV-defective mutant cells in the presence or absence of the same
279 FLC-subinhibitory concentration (0.6 μ g/mL). As expected³², FLC treatment led to lanosterol
280 accumulation in all strains under the growth conditions examined (**Fig 8D**). However, decreased
281 accumulation was observed in the *gat5Δ* and *hap2Δ* mutant strains as revealed by the ratio of
282 lanosterol/ergosterol signals, suggesting that the lipid composition is altered in these EV-defective
283 strains (**Fig 8E**).



284
285 **Figure 8:** Fluconazole treatment affects EV production and cellular sterol homeostasis. WT cells were grown in different
286 concentrations of FLC on SD agar medium, and the total number of cells was counted (A). Levels of *ERG11* expression in the
287 presence of a subinhibitory concentration of FLC (0.6 μ g/mL) (B). Analysis of EV production by nanoFCM in the presence of
288 FLC (0.6 μ g/mL) (C). Analysis of lanosterol and ergosterol lipid profile by thin layer chromatography, TLC in cells (D). Analysis
289 of TLC bands by densitometry units and ratio between lanosterol and ergosterol-specific signals for cells (E). The experiments
290 were carried out in at least two biological duplicates, and representative results were shown. Error bars show means \pm SD.

291
292 **g) FLC-resistant isolates obtained *in vitro* are impaired in EV production**
293 To further explore the link between FLC resistance and EV production in *C. neoformans*, we
294 analysed the EV production in spontaneous FLC-resistant isolates obtained *in vitro*. Previous studies
295 reported that when *C. neoformans* cells are spread on a medium containing an inhibitory FLC
296 concentration, a subset of the cell population can grow and produces colonies. This phenomenon is
297 known as heteroresistance and was associated with the duplication of chromosome 1 bearing *ERG11*
298 and *AFR1* resistance genes^{12,33,31}. This FLC-resistant phenotype can be reverted by subculturing the
299 cells in a drug-free medium, the phenotypic reversion being associated with the reversion of the

300 aneuploid genotype¹¹. Therefore, we isolated independent spontaneous FLC-resistant colonies on
301 plates containing 15 µg/mL of FLC. FLC-susceptible parental and FLC-resistant isolates were then
302 passaged six times in a liquid drug-free YPD. A schematic overview of the experimental design is
303 delineated in **Fig 9A**. All parental, resistant, and passage strains were tested for EV production and
304 FLC sensitivity. As expected, the sixteen passage 0 (P0) strains isolated on plates containing FLC were
305 resistant to FLC, as revealed by a significant decrease in the inhibition halo in FLC-disk diffusion assays
306 (**Fig 9B** and **9D**). Interestingly, this drug-resistant phenotype was accompanied by a substantial
307 reduction in EV production as analysed by nano-FCM (**Fig 9C**). Importantly, none of the sixteen FLC-
308 resistant isolates had pronounced growth defects in the SD medium, presenting the same transition
309 time frame from the exponential to stationary phase (**Fig S3**). In contrast, the passage 6 (P6) strains
310 all lost their resistant phenotype, although to a different extent (**Fig 9E** and **9G**), and they also restored
311 EV production to parental levels (**Fig 9F**).

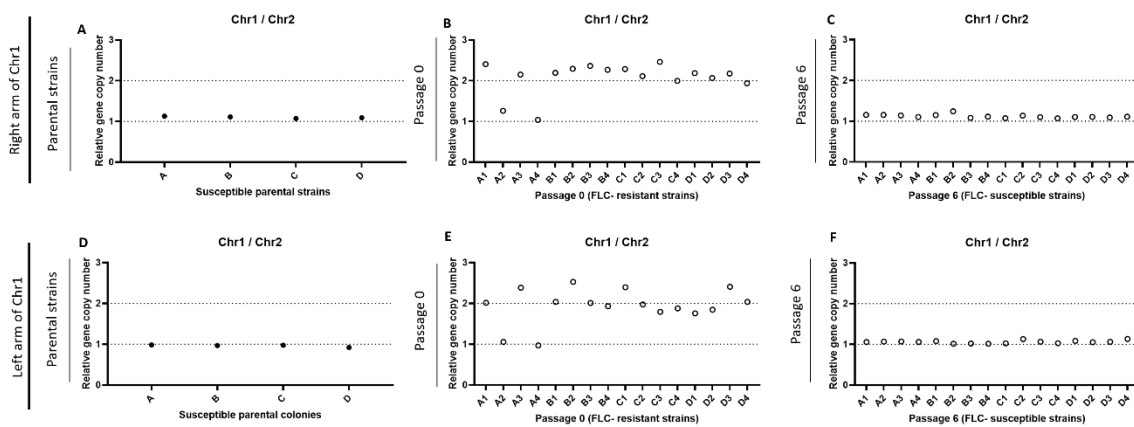


312

313 **Figure 9:** Analysis of FLC susceptibility and EV production in FLC-resistant isolates obtained *in vitro*. Illustrative scheme of the
314 experimental strategy used to explore the association between FLC resistance and EV production in spontaneous drug-
315 resistant strains obtained *in vitro* (A). Cells at passage 0: quantitative analysis of the growth inhibition halo from the FLC-disk
316 diffusion assays by diskImageR, RAD₈₀ (B), EV production analysis by nanoFCM (C), and qualitative analysis of the inhibition
317 halo of the FLC-disk diffusion assays (D). Cells after six successive passages in the absence of FLC: quantitative analysis of
318 growth inhibition halo from the FLC-disk diffusion assays by diskImageR, RAD₈₀ (E), EV production analysis by nanoFCM (F),
319 and qualitative analysis of the growth inhibition halo (G). Schematic representation created in BioRender.
320

321 We then evaluated the chromosome copy numbers of the parents, FLC-resistant, and
322 passed strains by qPCR (using primers for genes located on chromosome 1 left arm (CNAG_00047),
323 chromosome 1 right arm (CNAG_00483) and chromosome 2 (CNAG_03602)). As expected, all
324 parents were monosomic for chromosome 1 (**Fig 10A and 10D**). In agreement with the published

325 literature, we also found that fourteen out of sixteen FLC-resistant strains were disomic for
 326 chromosome 1 (**Fig 10B and 10E**). Meanwhile, all P6 strains reverted to the original monosomic state
 327 of chromosome 1 (**Fig 10C and 10F**).

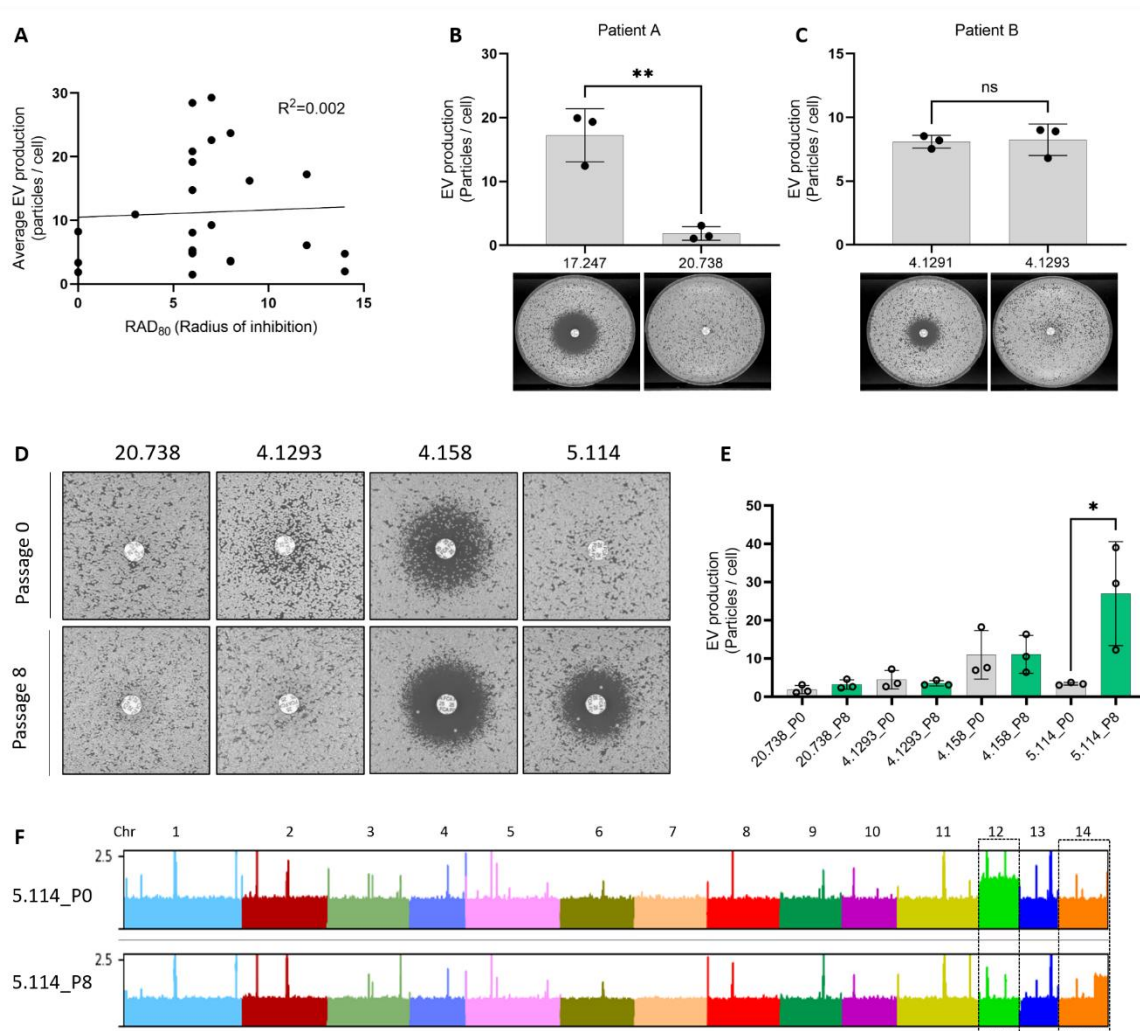


341 **Figure 11:** Chromosome duplications revealed after aligning DNA sequencing reads obtained from the A series of strains to
342 the *C. neoformans* reference genome (A). Analysis of *AFR1* (B) and *ERG11* (C) gene expression in A0, A2, and A4 strains by
343 RT-qPCR. Indicative of chromosome duplication (*).

344

345 **h) FLC resistance and regulation of EV release in *C. neoformans* clinical isolates**

346 To test whether the relationship between EV production and FLC resistance would extend to
347 clinical isolates, we studied a series of isolates having different levels of FLC susceptibility. Plotting the
348 the radius of inhibition (RAD_{80}) from FLC-disk diffusion assays and the average levels of EV production
349 from these isolates did not reveal a clear correlation ($R^2 = 0.002$), as both the fully resistant isolates
350 (no inhibition halo), as well as the most sensitive ones, were poor EV producers (**Fig 12A**). We then
351 considered serial isolates of *C. neoformans* that had become resistant during infection. For the isolates
352 CNRMA17.247 and CNRMA20.738, we observed that the acquisition of FLC resistance coincided with
353 the decreased ability to produce EVs (**Fig 12B**). For the second lineage (isolates CNRMA4.1291 and
354 CNRMA4.1293), we did not observe any difference in EV production between the sensitive and the
355 resistant isolates (**Fig 12C**). Interestingly, SNPs analysis revealed a CNRMA4.1293 specific (A to T)
356 nonsynonymous mutation in *ERG11*, responsible for a Y145F mutation and possibly associated with
357 the acquired resistance³⁴. We then tried to revert the resistance phenotype of four FLC-resistant
358 clinical isolates (CNRMA20.738, CNRMA4.1293, CNRMA4.158, and CNRMA5.114) by growing them in
359 a drug-free YPD medium for eight subsequent passages (P8). CNRMA5.114 was the only isolate for
360 which we obtained a more sensitive derivative (**Fig 12D**). In agreement with our previous observation,
361 the P8-sensitive passage produced more EVs than the original P0-resistant isolate (**Fig 12E**). As
362 expected, P8 strains with no change in drug susceptibility also did not display altered EV production
363 (**Fig 12D-E**). Sequencing the genomes of the two lineages of recurrent isolates as well as the P0 clinical
364 isolates and their P8 derivatives revealed no chromosomal duplications (**Fig S4**). Among the sequenced
365 P0 clinical isolates, we observed the disomy of chromosome 12 in CNRMA5.114, which was lost in its
366 P8 sensitive derivative. Partial duplication of chromosome 14 was also observed in the reverted P8
367 strain (**Fig 12F**). We did not further investigate a possible causative link between FLC resistance and
368 the observed genotype modifications in these isolates.



369
370 **Figure 12: EV production and FLC resistance are linked in clinical isolates.** Analysis of EV production by nanoFCM and size
371 of FLC-disk inhibition halo in clinical isolates by linear regression (A, radius of inhibition = RAD₈₀ values by diskImager). EV
372 production as measured by nanoFCM in the recurrent isolates CNRMA17.247 and CNRMA20.738 (top) and FLC-disk diffusion
373 assays (bottom) from patient A (B). EV production as measured by nanoFCM in the recurrent isolates CNRMA4.1291 and
374 CNRMA4.1293 (top) and FLC-disk diffusion assays (bottom) from patient B (C). FLC-disk diffusion assay in passaged clinical
375 isolates (D) and analysis of EV production of passaged clinical isolates by nanoFCM (E). Alignment of DNA-Seq reads obtained
376 from P0, and P8 CNRMA5.114 passaged clinical isolates (F). EV and FLC-disk analyses were carried out in at least biological
377 triplicates, and representative results were shown.

378
379 **3) Discussion**
380
381 The mechanisms of biogenesis of EVs in fungi are still unknown. In this paper, we present
382 experiments revealing a tight regulation of EV production in response to changes in growth conditions
383 in *C. neoformans*, confirming previous reports in other models^{35,36}. We also characterize four
384 transcription factor mutant strains strongly impaired in EV production which are the first to be
385 described in fungi and, to our knowledge, in any organisms. Surprisingly, we observed no major growth
386 defect associated with *hap2Δ* mutation, suggesting that a WT level of EV production is dispensable in
387 this fungus, at least under the examined conditions.

388 Our experiments also indicate that EV production is also strongly regulated by fungal growth
389 phase. EVs are produced between 16 h and 22 h after cell plating, corresponding to the transition
390 between the exponential phase and stationary phase. This result was consistent with reports of cells
391 growing on YPD solid medium³⁶. In *S. cerevisiae*, the transition from the exponential phase to the
392 stationary phase is associated with a shift from fermentation to respiration and a sharp slowdown of
393 the general metabolism^{37,38}. The Hap complex is the major regulator of this shift, controlling
394 respiration and mitochondrial function in this yeast^{39,40}. In pathogenic fungi, this complex has been
395 studied mostly for its regulatory function in iron metabolism^{41–43}. As in *S. cerevisiae*⁴⁴, the Hap complex
396 seems to control respiration in *C. neoformans*. Thus, Hap3 and HapX have also been shown to
397 negatively regulate genes encoding respiratory and TCA cycle function under low iron condition⁴⁵. The
398 *HAP* genes have also been shown to regulate sexual development in association with the pheromone-
399 responsive Cpk1 mitogen-activated protein kinase pathway in this pathogenic yeast⁴⁰. However,
400 phenotypic analyses of the *hap* mutants suggest that HapX and the Hap2/3/5 complex might also have
401 independent functions. For instance, *HAP3* and *HAP5* but not *HAPX* are necessary for growth on
402 ethanol⁴³, and the Hap2/3/5 complex, but not HapX, is crucial in repressing pheromone production
403 and cell fusion during mating⁴⁰. Similarly, we found that the Hap2/3/5 complex, but not HapX, controls
404 FLC resistance and EV production in *C. neoformans*.

405 The FLC resistance phenotype of the *hap* mutant strains is consistent with the literature^{45,62}.
406 Counterintuitively, Hap3 and HapX have been reported to positively regulate several ergosterol
407 biosynthetic genes⁴⁵. Our differential gene expression analysis, which used different growth
408 conditions, identified only two genes, *ERG20* (CNAG_02084) and *ERG27* (CNAG_07437)
409 downregulated and one upregulated, *IDI1* (CNAG_00265) upon *HAP2* deletion. Overall, these data
410 suggest that Hap2 in *C. neoformans* regulates global cellular changes impacting fluconazole resistance
411 beyond the regulation of the ergosterol pathway.

412 In this work, we present cumulative lines of evidence suggesting a causative link between FLC
413 resistance and EV production. First, all four EV production mutants displayed altered FLC susceptibility.
414 We also observed this association with other *hap* mutants; *hapxΔ* being the only one producing WT
415 level of EVs yet displaying a slight change in FLC susceptibility. Second, all spontaneous FLC-resistant
416 mutant strains isolated *in vitro* reduced the EV production, and both phenotypes reverted jointly. As
417 many spontaneous FLC mutant strains are disomic for chromosome 1 (known to bear *ERG11* and
418 *AFR1*¹²), one can imagine that repressors of EV production could also be located on this chromosome.
419 Thus, chromosome 1 disomy could increase the expression of both FLC-resistant genes and EV
420 repressors. However, we also identified two FLC-resistant spontaneous mutant strains with no

421 duplication of chromosome 1; one being disomic of chromosome 4. Interestingly, none of the EV
422 production regulators identified here are located on chromosome 1.

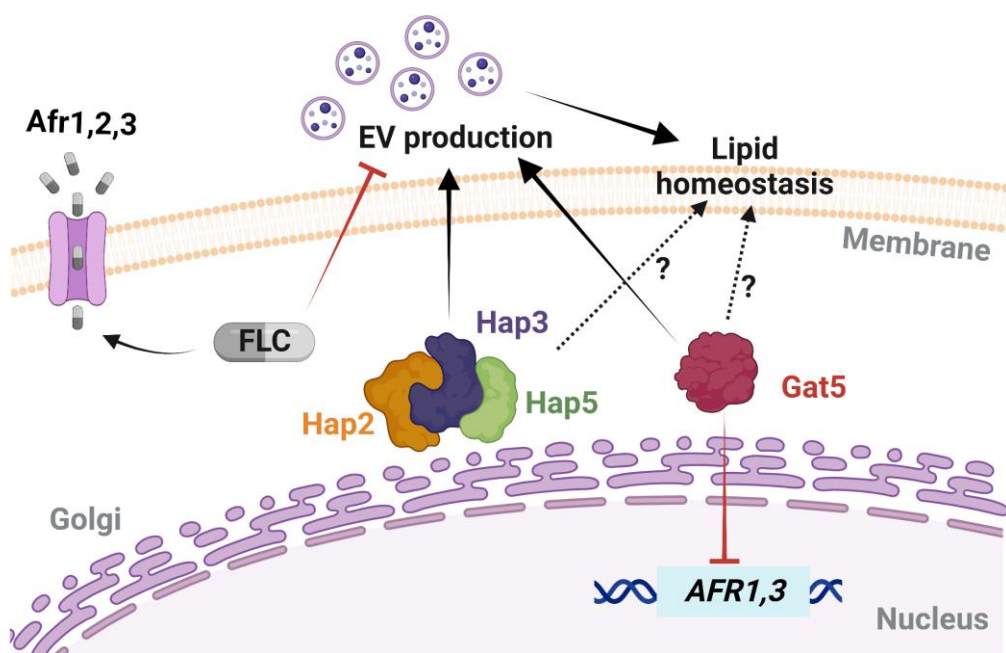
423 Finally, although we did not observe any correlations between the level of drug resistance and
424 EV production among clinical isolates, the analysis of a couple of serial isolates from the same patient
425 for which no mutation classically involved in FLC resistance could be identified revealed that the
426 resistant strain produced lower EV amounts compared to the sensitive one. Notably, we did not
427 observe any changes in chromosome copy numbers in these strains. Moreover, a sensitive strain
428 derived from a resistant clinical isolate obtained after several passages in a drug-free medium
429 produces more EVs than the original strain. This reinforces the idea that EV production and FLC
430 resistance are strongly linked, at least in a subset of genetic backgrounds.

431 Nevertheless, the molecular mechanism by which *Hap2* and *Gat5* regulate both EV production
432 and FLC susceptibility remains unknown. Overexpression of the drug efflux pumps *AFR1* and *AFR3* in
433 *gat5Δ* could contribute to the resistance phenotype. Similarly, disruption of the lanosterol/ergosterol
434 equilibrium in the presence of FLC in the EV-deficient mutants could also impact drug resistance.
435 Indeed, a recent report revealed that chemical disruption of the plasma homeostasis is sufficient to
436 modify azole resistance in pathogenic fungi⁴⁷. However, it is unclear whether the decreased EV
437 production alters plasma membrane homeostasis or whether these two TFs regulate membrane
438 homeostasis and, consequently, EV production. Previous data in *Cryptococcus* suggest that the
439 deletion of genes implicated in plasma membrane homeostasis can impact EV production and/or
440 cargo loading^{48,49}. On the other hand, the fact that most EV structural protein-encoding genes are
441 strongly downregulated in both *gat5Δ* and *hap2Δ* mutants suggests a direct effect of these TF on EV
442 biosynthesis. The fact that a Y145F *ERG11* mutation regulates FLC resistance without altering EV
443 production also favors this second hypothesis.

444 Interestingly, we found that a low concentration of FLC reduces EV production. Yet, this
445 concentration was not sufficient to alter the *ERG11* gene expression, suggesting that cells might
446 regulate EV production to maintain plasma membrane homeostasis. The impact of low antifungal
447 concentrations on fungal cell biology is poorly studied^{6,50}, but our data clearly indicates that fungal
448 cells might regulate EV production as a first line of defense under membrane stress. In this model (Fig
449 13), FLC exposure triggers distinct types of cellular responses; *ERG11* overexpression and EV
450 production would act to regulate plasma membrane homeostasis, whereas regulation of efflux pumps
451 would minimize FLC concentrations in the cell.

452 Overall, this study identified the first TF regulating fungal EV biosynthetic pathways, while also
453 uncovering novel roles that EVs play in modulating azole susceptibility. The genetics of EV production

454 is still in its infancy, but functional genetics will further our understanding of EV biogenesis, their
455 impact on drug resistance, and their roles during fungal infection.



456
457
458 **Figure 13:** Model of EV biogenesis regulation and FLC susceptibility in *C. neoformans*. Specific gene mutations and fluconazole
459 (FLC) exposure can trigger diverse cellular responses, including changes in the expressions of drug efflux-associated genes,
460 of the azole target gene, and in extracellular vesicles (EV) biogenesis. Gat5 inhibits the expression of *AFR1* and *AFR3*, which
461 can affect the intracellular FLC levels, while sub-inhibitory concentration of FLC can inhibit EV production. Hap2/3/5 and Gat5
462 regulate EV production, and cellular lipid homeostasis. The differential regulation of these cellular processes may determine
463 FLC resistance phenotypes in this fungal pathogen. Schematic model created in BioRender.
464
465

466 4) Methods

467 Media and culture conditions.

468 All strains were taken from the G. Janbon laboratory collection at -80°C, plated onto yeast peptone
469 dextrose (YPD) agar plates (1% yeast extract, 2% bacto-peptone, 2% dextrose, 2% bacto-agar) and
470 incubated at 30°C for 48h before each experiment. Cell inoculum was performed in broth YPD (1%
471 yeast extract, 2% bacto-peptone, 2% dextrose) rotating at 180 rpm for 24h at 30°C. The other solid
472 media used in this study included Sabouraud (SAB) containing 1% bacto-peptone, 4% dextrose, 2%
473 bacto-agar, Synthetic dextrose (SD) containing 0.67% yeast nitrogen base (Difco) without amino acids,
474 2% glucose and 2% bacto-agar; and Capsule induction medium (IM) containing 1.7 g of yeast nitrogen
475 base without amino acids and without ammonium sulfate (Difco), 1.5 g of asparagine and 20 g of
476 glucose L⁻¹ of buffer (12mM in NaHCO₃, 35mM in MOPS, pH 7.1), as previously described⁵¹. Drug-
477 containing plates were made by adding a stock solution of 3 mg/mL FLC powder in water to different

478 final concentrations depending on each experiment. The drug was added to the agar after autoclaving,
479 then cooled to approximately 50°C before pouring.

480

481 **Fungal strains and mutant construction**

482 The *C. neoformans* TF mutant library²⁶ was obtained from the Fungal Genetic Stock Center (USA). This
483 collection has been constructed in an H99o background⁵². After the screening, the phenotype of the
484 identified EV mutant strains was thus confirmed in the KN99α⁵³ background. All the following
485 experiments have been performed in KN99α reference background⁵². The strains used are listed in
486 **Supplementary Table S2**. The strains *MATα hap2Δ::NAT* (CNAG_07435), *MATα hap3Δ::NAT*
487 (CNAG_02215), *MATα hap5Δ::NAT* (CNAG_07680), *MATα hapXΔ::NAT* (CNAG_01242), *MATα*
488 *gat5Δ::NAT* (CNAG_05153), *MATα nrg1Δ::NAT* (CNAG_05222) have been constructed in the Hiten
489 Madhani lab (UCSF, USA) and obtained from the Fungal Genetic Stock Center. The genotypes of these
490 mutant strains were confirmed by PCR using gene-specific internal primers. To construct the strains
491 NE1539 (*MATα bzp2Δ::NAT*) and NE1540 (*MATα liv4Δ::NAT*), we replaced the entire CNAG_04263
492 (*BZP2*) and CNAG_06283 (*LIV4*) CDS by the NAT marker. The deletion cassettes construction and
493 transformant screening were performed as previously described³³. The *GAT5* and *HAP2* genes were
494 re-introduced into the corresponding mutant strain using a transient CRISPR-Cas9 expression (TRACE)
495 system⁵⁴. DNA fragments spanning a genomic region from 1kb upstream to 1kb downstream the CDS
496 of the genes were PCR amplified and cloned into the pSDMA57 plasmid before being integrated at the
497 genomic “safe haven” locus in *gat5Δ* and *hap2Δ* mutants, respectively⁵⁵. All plasmids and primer
498 sequences used are provided in **Supplementary Tables S3 and S4**, respectively. Twenty-four clinical
499 isolates of *C. neoformans* were also used. All isolates were recovered from the national cryptococcosis
500 surveillance program managed by the National Reference Center for Invasive Mycoses & Antifungals
501 (NRCMA, Institut Pasteur) between 2004 and 2021. All the clinical isolates are provided in
502 **Supplementary Table S2**.

503

504 **EV isolation protocol and optimization for EV screening in 96-well plates**

505 EV isolation by the conventional ultracentrifugation method followed the steps of the previously
506 described protocol¹⁴. A 96-format protocol was also used to test a large number of samples
507 concomitantly. For this, cells from the stock were streaked on YPD agar plates for 48h at 30°C, and
508 one loop of cells was inoculated in 1 ml of YPD broth of each well of a 96-deep well plate and incubated
509 for 18h at 30°C under agitation. The plate was centrifuged, and cells were washed twice with sterile
510 water, adjusted to OD₆₀₀ = 0.4 using a Tecan microplate reader (Tecan Trading AG, Switzerland). Then,
511 300 µL of the cell suspension was spread onto SD agar plates. After incubation for 24h at 30°C, cells

512 were gently recovered from the agar plates with an inoculation loop and suspended in 1 mL of 0.22
513 μm -filtered PBS 1x in 2 mL Eppendorf tubes by pipetting up and down. The total number of cells
514 collected from plates was evaluated by Coulter Counter (Z series, Beckman). Cells were centrifuged
515 for 5 min at 7,000 $\times g$; the supernatant was collected in a 1.5ml tube and centrifuged again at 11,000
516 $\times g$ for 5 min. Supernatants were transferred to 96-well filter plates with 0.45 μm pore size and
517 centrifuged at 2,500 $\times g$ for 3 min at 4°C. The filtered supernatants were kept at -80°C for further
518 evaluations, including the quantification of EV single particles and EV size diameter by the Flow
519 Nanoanalyser⁵⁶ (nanoFCMTM) and/or by measuring the total sterol amount by AmplexTM Red
520 Cholesterol Assay Kit (ThermoFisher, A12216), following manufacturer's instructions.

521 In the TF mutant collection²⁵, each mutant is present as two or three independently obtained
522 strains. Here, we first tested one mutant per gene. We then selected the most promising candidates
523 producing less than 0.5-fold or more than 1.5-fold EVs compared to the WT strain. We then tested the
524 second and third independent mutants when available in the collection. For all the mutants tested,
525 the EV production was measured by the total amount of sterol normalized by the total number of cells
526 collected for each strain. For the mutant strain 3.C10 (*gat1Δ*), which did not grow on SD plates, the EV
527 production ratio was calculated based on mutant and WT growth on YPD agar plates.

528

529 **Quantification of EV particles by nanoFCM**

530 A NanoAnalyzer (nanoFCM) instrument equipped with a 488 nm laser at 50 mW and single-photon
531 counting avalanche photodiodes detectors (SPCM APDs) was used for the detection of the EV
532 particles. Band-pass filters allowed for the collection of light in specific channels (488/10 nm). Light
533 scattering and fluorescence of individual EVs were collected on single-photon counting avalanche
534 photodiodes detectors on three channels: side scatter (SSC) - 488/10 (trigger channel). Sample fluid
535 was focused to approximately 1.4 μm using an HPLC-grade water filter and de-gas as the sheath fluid
536 via gravity feed. Data were generated through the Nanoanalyser Professional Suite V 2.0 software,
537 0.02 μm - filtered PBS was used to define the event triggering threshold. Measurements were taken
538 over one-minute periods at a sampling pressure of approximately 1.0 kPa, modulated, and maintained
539 by an air-based pressure module. Samples were diluted in 0.02 μm - filtered PBS as required to allow
540 3,000 to 13,000 counts to be recorded during this time. During data acquisition, the sample stream is
541 completely illuminated within the central region of the focused laser beam, resulting in approximately
542 100% detection efficiency, which leads to accurate particle concentration measurement via single-
543 particle enumeration. Optical alignment was tested and calibrated using fluorescent 250 nm silica
544 nanoparticles. Further calibration measurements were taken prior to analysis using 250 nm silica
545 nanoparticles of known concentration (for EV concentration calculation). Isolated EV samples were

546 sized according to standard operating procedures using the proprietary 4-modal silica nanosphere
547 cocktail generated by nanoFCM to allow for a standard curve to be generated based on the four sizes
548 of the nanosphere populations of 68 nm, 91 nm, 113 nm, and 155 nm in diameter. Silica provides a
549 stable and monodisperse standard with a refractive index of approximately 1.43 to 1.46, which is close
550 to the range of refractive indices reported in the literature for EVs ($n = 1.37$ to 1.42). Using such a
551 calibration standard enabled accurate flow cytometry size measurements, as confirmed when
552 comparing flow cytometry with cryo-TEM results. The laser was set to 10 mW and 10% SSC decay.
553 Data reported in the figure were handled within the nanoFCM Professional Suite v2.0 software to
554 analyse particles between 40 nm and 155 nm.

555

556 **DNA and RNA purification and sequencing libraries preparation**

557 *C. neoformans* KN99a, *hap2Δ*, and *gat5Δ* strains were grown in EV production condition on SD for 18h
558 at 30°C. Cells were collected from the agar plates and suspended in 10ml 0.22μm-filtered PBS 1x. RNA
559 extracts were prepared as previously described^{57,58}. Each condition was used to prepare biological
560 triplicate samples. RNA-seq analysis was performed as previously described⁵⁹. Briefly, strand-specific,
561 paired-end cDNA libraries were prepared from 1.5 μg of total RNA by polyA selection using the TruSeq
562 Stranded mRNA kit (Illumina) according to the manufacturer's instructions. cDNA fragments of ~400
563 bp were purified from each library and confirmed for quality by Bioanalyzer (Agilent). DNA-Seq
564 libraries from 2.5 μg of genome DNA were prepared using the TruSeq DNA PCR-free kit (Illumina).
565 Then, 100 bases were sequenced from both ends using an Illumina NextSeq500 instrument according
566 to the manufacturer's instructions (Illumina).

567

568 **Sequencing library trimming and mapping**

569 The paired reads from the RNA-seq libraries were trimmed for low-quality reads, and Illumina TruSeq
570 adapters were removed with Cutadapt v1.9.1 (<https://doi.org/10.14806/ej.17.1.200>) with the
571 following parameters: --trim-qualities 30 --e (maximum error rate) 0.1 --times 3 --overlap 6 --
572 minimum-length 30. The cleaning of rRNA sequences was performed with Bowtie2 v2.3.3⁶⁰ with
573 default parameters; unmapped paired reads were reported using option --un-conc to identify reads
574 that did not align with rRNA sequences. The cleaned reads from RNA-seq paired-end libraries from *C.*
575 *neoformans* to the H99 reference genome (NCBI Genome Assembly GCA_000149245.3) with Tophat2
576 v2.0.14⁶¹ and the following parameters: minimum intron length 30; minimum intron coverage 30;
577 minimum intron segment 30; maximum intron length 4000; maximum multihits 1; microexon search.
578 Analysis of differential expression data was performed in DeSeq2⁶².

579 DNA read alignment, variant detection, and ploidy analysis were performed as previously described
580 ⁶³. Illumina reads were aligned to the *C. neoformans* H99 reference genome using Minimap2 aligner
581 v.2.9⁶⁴ with the "-ax sr" parameter. BAM files were sorted and indexed using SAMtools⁶⁵ version 1.9.
582 Picard version 2.8.1 (<http://broadinstitute.github.io/picard>) tools were used to identify duplicate
583 reads and assign correct read groups to BAM files. SAMtools version 1.9 and Picard version 2.8.1 were
584 then used to filter, sort, and convert SAM files and assign read groups, and mark duplicate reads.
585 Single-nucleotide polymorphisms (SNPs) and insertions/deletions (indels) were called using Genome
586 Analysis Toolkit version 3.6 with ploidy=1 according to the GATK Best Practices. HaploScore
587 parameters used to filter SNPs and indels included VariantFiltration, QD <2.0, LowQD,
588 ReadPosRankSum<-8.0, LowRankSum, FS >60.0, HightFS, MQRankSum<-12.5, MQRankSum, MQ
589 <40.0, LowMQ, and HaplotypeScore >13.0. To examine variations in ploidy across the genome, the
590 sequencing depth at all positions was computed using SAMtools⁶⁵, and then the average depth was
591 computed for 1-kb windows across the genome. Gene ontology (GO) analyses were performed using
592 the FungiDB database (<https://fungidb.org/fungidb/app>).

593

594 **Obtention of FLC-resistant *in vitro* strains and passaged derivatives**

595 To obtain FLC-resistant *C. neoformans* strains *in vitro*, WT KN99α cells, previously grown for 24h at
596 30°C, were plated on drug-free YPD agar plates and incubated for 48h at 30°C. Four isolated parental
597 colonies were used to inoculate four YPD liquid cultures grown ON at 30°C. An aliquot of the cells was
598 stored at -80°C, and 1 ml of the culture was washed once with sterile water and adjusted to 10⁵
599 cells/mL. 200 µL of the cell suspension was plated on new YPD plates supplemented with FLC at
600 15µg/mL and incubated for five days at 30°C. Four independent FLC-resistant colonies for each initial
601 parental culture were collected from the plates, totalizing 16 resistant isolates. Each of these 16 strains
602 was cultured in liquid YPD drug-free medium ON before being stored at -80°C (P0 isolates). For the
603 culture passages, susceptible parental cells and FLC-resistant derived strains were thawed on YPD agar
604 plates (30°C) for 48h. One small loop of the cells was inoculated in 1 mL of YPD in 96 deep well plates
605 that were incubated under rotation at 30°C. Every 48h days, 10 µL of the cell suspension was collected
606 and inoculated in 990 µL of fresh YPD using a multichannel. The remaining cells from each passage
607 were centrifuged at 4000 x rpm for 5 min (4°C), the supernatant was discarded, and the cell pellet was
608 suspended in 200 µL of glycerol (40%) for keeping at - 80°C. Parental strains and 96 well plates
609 containing cells from passages 1 to 6 were stored at -80°C and further used for EV isolation and FLC-
610 disk assays.

611

612 **Disk diffusion and spot assays**

613 Disk diffusion assays were performed as previously described⁴², with minor adjustments. Cells were
614 grown for 24h in YPD broth at 30°C under agitation, centrifuged, washed once in sterile PBS 1x, and
615 diluted at 1×10^6 cells/mL. 100 μ L of the cell suspension was spread onto YPD agar plates. A single 25
616 μ g FLC disk (BioRad) was placed in the center of each plate. Plates were incubated at 30 °C for 48 h
617 and 72 h and photographed individually using a PhenoBooth+ (Singer Instrument, USA) apparatus.
618 Analysis of the disk diffusion assay was done by ImageJ or by using the diskImageR pipeline, as
619 previously described⁵⁶. Radius of inhibition levels, referred to as RAD throughout the manuscript,
620 represents parameters measured at 80% drug inhibition (RAD₈₀). Cells for spot assays were prepared
621 following the same steps previously described. Cells were diluted to 1×10^7 cells/mL and spotted (3
622 μ l) in 10-fold serial dilutions onto the YPD plates containing the different drugs and compounds. The
623 susceptibility assays were repeated a minimum of two times.

624

625 **RT-qPCR for *ERG11*, *AFR1*-*AFR3* expression, and chromosomal ploidy analysis**

626 For the analysis of gene expression by qPCR, three independent samples were prepared for each strain
627 (WT, *hap2Δ*, *gat5Δ*, and *nrg1Δ*). Cells were cultured in YPD for 18 h at 30°C, under agitation. Then, 6.4
628 $\times 10^8$ cells were transferred to 100 mL of YPD and grown for 4h, at 30°C, under agitation. After the 4 h
629 incubation, FLC was added at a final concentration of 10 μ g/mL. We skipped this step in the control.
630 Cell cultures were incubated for 2 additional hours at 30°C under agitation. Cells were counted and
631 washed once with sterile water, and pellets were kept at -80°C for further RNA extraction, as
632 previously described³⁵. Purified RNA was treated with DNase I recombinant, RNase-free (Roche) to
633 eliminate residual genomic DNA. Synthesis of cDNA was performed using the Thermo Scientific
634 Maxima First Strand cDNA Synthesis Kit for RT-qPCR, following the manufacturer's instructions. The
635 expression levels of *ERG11* and *AFR1*-*AFR3* genes were determined by qPCR using 5 μ l of the
636 appropriate dilutions of cDNA and 1 μ L of each primer of interest (10 μ M), listed in **Supplementary**
637 **Table S4**. The reactions were performed using the SsoAdvanced Universal SYBR Green Supermix in
638 Hard Shell qPCR plate 96-well thin wall (Bio-Rad). Amplification reactions were performed using an
639 RT-PCR Detection System thermal cycler (Bio-Rad). The Ct values obtained in triplicates were
640 averaged, and the number of molecules measured by standard curves and normalized to that of the
641 housekeeping gene *ACT1* (CNAG_00483). All RT-qPCR data were from three biological replicates (three
642 independent RNA preparations).
643 We used qPCR assays and primers specific to the genes CNAG_00483, CNAG_00047, and CNAG_03602
644 to evaluate the copy number of the chromosome 1 right harm, chromosome 1 left harm, and
645 chromosome 2, respectively (**Supplementary Table S4**).
646

647 **Lipid analysis by thin layer chromatography**

648 Cells collected after 24h grown on SD agar plates with or without FLC (0.6 μ g/mL) were suspended in
649 a mixture of chloroform (C) and methanol (M), C/M (2:1 [vol/vol]) and incubated for 4h at room
650 temperature. The suspension was clarified by centrifugation, and the supernatants were stored. Cell
651 pellets were again extracted with a mixture of C and M (1:2 [vol/vol]) under the same conditions.
652 Supernatants containing the lipid extracts were combined and dried using a rotavapor (Heidolph,
653 Germany). The resulting cell lipid extracts were submitted to a partition system composed of
654 C/M/0.75% KCl in water (8:4:3 [vol/vol/vol]) and vigorously mixed. The lower phase was dried under
655 a N₂ stream, weighed, and suspended in C to reach a concentration of 10 mg/mL of total cellular lipid
656 extracted. To analyze cellular lipids, 50 μ g of total lipid was spotted into thin layer chromatography
657 (TLC) plates (silica gel 60 F₂₅₄; Merck, Germany). A total of 3 μ L of purified Lanosterol and Ergosterol
658 (1mg/mL) were spotted in TLC plates as running standards. The plates were developed in chambers
659 pre-saturated for 10 min at room temperature using cyclohexane and ethyl acetate (3:2 [vol/vol] as a
660 solvent running system. Plates were sprayed with a solution of 50 mg ferric chloride (FeCl₃) in a
661 mixture of 90 mL water, 5 mL acetic acid, and 5 mL sulfuric acid. After heating at 100 °C for 3–5 min,
662 the sterol spots were identified by the appearance of a red-violet color. TLC plates were imaged, and
663 the bands were densitometrically analysed using Image J (NIH, USA). Values were expressed as ratios
664 between cellular lanosterol and ergosterol-specific levels.

665

666 **Statistical analysis**

667 All statistical analyses were performed using GraphPad Prism 9 software (GraphPad Software Inc.).
668 Data sets were tested for normal distribution using Shapiro-Wilk or Kolmogorov-Smirnov normality
669 tests. In the cases in which the data passed the normality test, they were further analysed using the
670 unpaired Student's t test or ordinary one-way ANOVA. When at least one data set was nonnormally
671 distributed, we used the nonparametric Kolmogorov-Smirnov or Kruskal-Wallis test.

672

673 **Availability and accession number**

674 Raw data are available at Bioproject: PRJNA928602

675 **5) Acknowledgments**

676 JR was supported by the Pasteur-Roux-Cantarini fellowship of Institut Pasteur and by FAPERJ -
677 Fundação de Amparo à Pesquisa do Estado do Rio de Janeiro (E-26/204.456/2021). This work was
678 supported by a CAPES COFECUB grant n°39712ZK to GJ, MLR, and LN. The work was supported by an
679 ANR grant (Projet ResistEV AAPG2021 CE35) to GJ, IVE and AA, T.T.V.D was supported by the Pasteur -
680 Paris University (PPU) International PhD Program. IVE is supported by a CIFAR Azrieli Global Scholar

681 Award. We would like to thank in particular Laëtitia Viengsavanah for the help with the initial steps of
682 TF mutant collection screening, and some members of the French Cryptococcosis Study Group:
683 Christine Bonnal (Hôpital Bichat-Claude Bernard Paris), Marie-Elisabeth Bougnoux (Hôpital Necker-
684 Enfants Malades, Paris), Nathalie Bourgeois (CHU Montpellier), Sophie Cassaing (CHU Toulouse), Lilia
685 Hasseine (CHU Nice), and Stéphane Ranque (IHU Méditerranée Infection, Marseille).

686

687 **6) Author contributions**

688 J.R., A.T., and F.M. performed the transcription factor mutant library screening for EV production, drug
689 susceptibility assays, isolation of *in vitro* clinical isolates, growth passages and RT-qPCR analyses. F.M.
690 and I.M. helped with the mutant construction. J.Y.C. and JR prepared the DNA and RNA sequencing
691 libraries. C.M. performed the sequencing library trimming, mapping and bioinformatic analyses. P.C.
692 and S.N. helped with the nanoflow cytometry analyses. I.V.E. advised on drug susceptibility assays and
693 experimental design. G.P.A. performed cryo-electron microscopy analyses. L.N. and A.G.Z. performed
694 the lipid analysis. T.T.V.D. and J.R. performed the gene complementations. A.A and M.D. selected the
695 clinical strains to be studied. J.R. and G.J. conceived and designed the project. G.J. and M.L.R.
696 supervised the research. J.R. and G.J. wrote the manuscript. All authors commented on the final
697 version. All authors have read and agreed to the published version of the manuscript.

698

699 **7) References**

700

- 701 1. Fisher, M. C. *et al.* Threats Posed by the Fungal Kingdom to Humans, Wildlife, and Agriculture.
702 *mBio* **11**, e00449-20 (2020).
- 703 2. Janbon, G., Quintin, J., Lanternier, F. & d'Enfert, C. Studying fungal pathogens of humans and
704 fungal infections: fungal diversity and diversity of approaches. *Genes Immun* **20**, 403–414 (2019).
- 705 3. Brown, G. D. *et al.* Hidden killers: human fungal infections. *Science translational medicine* **4**,
706 165rv13 (2012).
- 707 4. WHO fungal priority pathogens list to guide research, development and public health action.
708 <https://www.who.int/publications-detail-redirect/9789240060241>.
- 709 5. Rajasingham, R. *et al.* Global burden of disease of HIV-associated cryptococcal meningitis: an
710 updated analysis. *The Lancet Infectious Diseases* **17**, 873–881 (2017).

711 6. Fisher, M. C. *et al.* Tackling the emerging threat of antifungal resistance to human health. *Nat Rev Microbiol* **20**, 557–571 (2022).

712

713 7. Almeida, F., Rodrigues, M. L. & Coelho, C. The Still Underestimated Problem of Fungal Diseases

714 Worldwide. *Frontiers in Microbiology* **10**, (2019).

715 8. Robbins, N., Caplan, T. & Cowen, L. E. Molecular Evolution of Antifungal Drug Resistance. *Annu Rev Microbiol* **71**, 753–775 (2017).

716

717 9. Berman, J. & Krysan, D. J. Drug resistance and tolerance in fungi. *Nat Rev Microbiol* **18**, 319–331

718 (2020).

719 10. Rodero, L. *et al.* G484S Amino Acid Substitution in Lanosterol 14- α Demethylase (ERG11) Is

720 Related to Fluconazole Resistance in a Recurrent *Cryptococcus neoformans* Clinical Isolate.

721 *Antimicrobial Agents and Chemotherapy* **47**, 3653–3656 (2003).

722 11. Sionov, E., Lee, H., Chang, Y. C. & Kwon-Chung, K. J. *Cryptococcus neoformans* Overcomes

723 Stress of Azole Drugs by Formation of Disomy in Specific Multiple Chromosomes. *PLOS Pathogens*

724 **6**, e1000848 (2010).

725 12. Stone, N. R. H. *et al.* Dynamic ploidy changes drive fluconazole resistance in human

726 cryptococcal meningitis. *Journal of Clinical Investigation* **129**, 999–1014 (2019).

727 13. Rizzo, J., Rodrigues, M. L. & Janbon, G. Extracellular Vesicles in Fungi: Past, Present, and

728 Future Perspectives. *Front. Cell. Infect. Microbiol.* **10**, 346 (2020).

729 14. Rizzo, J. *et al.* *Cryptococcus* extracellular vesicles properties and their use as vaccine

730 platforms. *Journal of Extracellular Vesicles* **10**, (2021).

731 15. Zhao, M. *et al.* Turbinmicin inhibits *Candida* biofilm growth by disrupting fungal vesicle–

732 mediated trafficking. *Journal of Clinical Investigation* **131**, e145123 (2021).

733 16. Demuyser, L., Van Dyck, K., Timmermans, B. & Van Dijck, P. Inhibition of Vesicular Transport

734 Influences Fungal Susceptibility to Fluconazole. *Antimicrob Agents Chemother* **63**, e01998-18

735 (2019).

736 17. Estrada, A. F., Muruganandam, G., Prescianotto-Baschong, C. & Spang, A. The ArfGAP2/3
737 Glo3 and ergosterol collaborate in transport of a subset of cargoes. *Biol Open* **4**, 792–802 (2015).

738 18. Walton, F. J., Heitman, J. & Idnurm, A. Conserved elements of the RAM signaling pathway
739 establish cell polarity in the basidiomycete *Cryptococcus neoformans* in a divergent fashion from
740 other fungi. *Mol Biol Cell* **17**, 3768–3780 (2006).

741 19. Wambaugh, M. A. *et al.* Synergistic and antagonistic drug interactions in the treatment of
742 systemic fungal infections. *Elife* **9**, e54160 (2020).

743 20. Zarnowski, R. *et al.* *Candida albicans* biofilm-induced vesicles confer drug resistance through
744 matrix biogenesis. *PLoS Biol* **16**, e2006872 (2018).

745 21. Chan, W. *et al.* Induction of amphotericin B resistance in susceptible *Candida auris* by
746 extracellular vesicles. *Emerging Microbes & Infections* **11**, 1900–1909 (2022).

747 22. Zarnowski, R. *et al.* Coordination of fungal biofilm development by extracellular vesicle
748 cargo. *Nat Commun* **12**, 6235 (2021).

749 23. Zhao, K. *et al.* Extracellular vesicles secreted by *Saccharomyces cerevisiae* are involved in cell
750 wall remodelling. *Commun Biol* **2**, 1–13 (2019).

751 24. Douanne, N. *et al.* Leishmania parasites exchange drug-resistance genes through
752 extracellular vesicles. *Cell Reports* **40**, 111121 (2022).

753 25. Jung, K.-W. *et al.* Systematic functional profiling of transcription factor networks in
754 *Cryptococcus neoformans*. *Nat Commun* **6**, 6757 (2015).

755 26. Cui, W., Li, X., Hull, L. & Xiao, M. GATA-type transcription factors play a vital role in radiation
756 sensitivity of *Cryptococcus neoformans* by regulating the gene expression of specific amino acid
757 permeases. *Sci Rep* **9**, 6385 (2019).

758 27. Yi, J. *et al.* Transcription factor Liv4 is required for growth and pathogenesis of *Cryptococcus*
759 *neoformans*. *FEMS Yeast Research* **20**, foaa015 (2020).

760 28. Mao, Y. & Chen, C. The Hap Complex in Yeasts: Structure, Assembly Mode, and Gene
761 Regulation. *Front. Microbiol.* **10**, 1645 (2019).

762 29. Fuge, E. K., Braun, E. L. & Werner-Washburne, M. Protein synthesis in long-term stationary-
763 phase cultures of *Saccharomyces cerevisiae*. *J Bacteriol* **176**, 5802–5813 (1994).

764 30. Gow, N. A. R. *et al.* The importance of antimicrobial resistance in medical mycology. *Nat
765 Commun* **13**, 5352 (2022).

766 31. Jordá, T. & Puig, S. Regulation of Ergosterol Biosynthesis in *Saccharomyces cerevisiae*. *Genes
(Basel)* **11**, 795 (2020).

768 32. Foresti, O., Ruggiano, A., Hannibal-Bach, H. K., Ejsing, C. S. & Carvalho, P. Sterol homeostasis
769 requires regulated degradation of squalene monooxygenase by the ubiquitin ligase Doa10/Teb4.
770 *Elife* **2**, e00953 (2013).

771 33. Mondon, P. *et al.* Heteroresistance to fluconazole and voriconazole in *Cryptococcus
772 neoformans*. *Antimicrob Agents Chemother* **43**, 1856–1861 (1999).

773 34. Sionov, E. *et al.* Identification of a *Cryptococcus neoformans* Cytochrome P450 Lanosterol
774 14 α -Demethylase (Erg11) Residue Critical for Differential Susceptibility between
775 Fluconazole/Voriconazole and Itraconazole/Posaconazole | Antimicrobial Agents and
776 Chemotherapy. <https://journals.asm.org/doi/10.1128/AAC.05502-11>.

777 35. Cleare, L. G. *et al.* Media Matters! Alterations in the loading and release of *Histoplasma
778 capsulatum* extracellular vesicles in response to different nutritional milieus. *Cellular
779 Microbiology* **n/a**, e13217.

780 36. Reis, F. C. G. *et al.* Analysis of Cryptococcal Extracellular Vesicles: Experimental Approaches
781 for Studying Their Diversity Among Multiple Isolates, Kinetics of Production, Methods of
782 Separation, and Detection in Cultures of Titan Cells. *Microbiol Spectr* **9**, e0012521 (2021).

783 37. Werner-Washburne, M., Braun, E., Johnston, G. C. & Singer, R. A. Stationary phase in the
784 yeast *Saccharomyces cerevisiae*. *Microbiol Rev* **57**, 383–401 (1993).

785 38. Galdieri, L., Mehrotra, S., Yu, S. & Vancura, A. Transcriptional regulation in yeast during
786 diauxic shift and stationary phase. *OMICS* **14**, 629–638 (2010).

787 39. S, B. *et al.* The *S. Cerevisiae* HAP complex, a key regulator of mitochondrial function,
788 coordinates nuclear and mitochondrial gene expression. *Comparative and functional genomics* **4**,
789 (2003).

790 40. Bolotin-Fukuhara, M. Thirty years of the HAP2/3/4/5 complex. *Biochim Biophys Acta Gene
791 Regul Mech* **1860**, 543–559 (2017).

792 41. Singh, R. P., Prasad, H. K., Sinha, I., Agarwal, N. & Natarajan, K. Cap2-HAP complex is a critical
793 transcriptional regulator that has dual but contrasting roles in regulation of iron homeostasis in
794 *Candida albicans*. *J Biol Chem* **286**, 25154–25170 (2011).

795 42. Gsaller, F. *et al.* The Janus transcription factor HapX controls fungal adaptation to both iron
796 starvation and iron excess. *EMBO J* **33**, 2261–2276 (2014).

797 43. Jung, W. H. *et al.* HapX positively and negatively regulates the transcriptional response to
798 iron deprivation in *Cryptococcus neoformans*. *PLoS Pathog* **6**, e1001209 (2010).

799 44. Buschlen, S. *et al.* The *S. Cerevisiae* HAP complex, a key regulator of mitochondrial function,
800 coordinates nuclear and mitochondrial gene expression. *Comp Funct Genomics* **4**, 37–46 (2003).

801 45. Kim, J. *et al.* A defect in iron uptake enhances the susceptibility of *Cryptococcus neoformans*
802 to azole antifungal drugs. *Fungal Genet Biol* **49**, 955–966 (2012).

803 46. Caza, M., Hu, G., Price, M., Perfect, J. R. & Kronstad, J. W. The Zinc Finger Protein Mig1
804 Regulates Mitochondrial Function and Azole Drug Susceptibility in the Pathogenic Fungus
805 *Cryptococcus neoformans*. *mSphere* **1**, e00080-15 (2016).

806 47. Revie, N. M. *et al.* Targeting fungal membrane homeostasis with imidazopyrazoindoles
807 impairs azole resistance and biofilm formation. *Nat Commun* **13**, 3634 (2022).

808 48. Reis, F. C. G. *et al.* A Novel Protocol for the Isolation of Fungal Extracellular Vesicles Reveals
809 the Participation of a Putative Scramblase in Polysaccharide Export and Capsule Construction in
810 *Cryptococcus gattii*. *mSphere* **4**, (2019).

811 49. Rizzo, J. *et al.* Role of the Apt1 protein in polysaccharide secretion by *Cryptococcus
812 neoformans*. *Eukaryotic cell* **13**, 715–26 (2014).

813 50. Handelman, M. & Osherov, N. Experimental and in-host evolution of triazole resistance in
814 human pathogenic fungi. *Frontiers in Fungal Biology* **3**, (2022).

815 51. Janbon, G., Himmelreich, U., Moyrand, F., Improvisi, L. & Dromer, F. Cas1p is a membrane
816 protein necessary for the O-acetylation of the *Cryptococcus neoformans* capsular polysaccharide.
817 *Molecular Microbiology* **42**, 453–467 (2001).

818 52. Janbon, G. *et al.* Analysis of the Genome and Transcriptome of *Cryptococcus neoformans*
819 var. grubii Reveals Complex RNA Expression and Microevolution Leading to Virulence
820 Attenuation. *PLoS Genet* **10**, e1004261 (2014).

821 53. Nielsen, K. *et al.* Sexual cycle of *Cryptococcus neoformans* var. grubii and virulence of
822 congeneric a and alpha isolates. *Infect Immun* **71**, 4831–4841 (2003).

823 54. Lin, J., Fan, Y. & Lin, X. Transformation of *Cryptococcus neoformans* by electroporation using
824 a transient CRISPR-Cas9 expression (TRACE) system. *Fungal Genet Biol* **138**, 103364 (2020).

825 55. Arras, S. D. M., Chitty, J. L., Blake, K. L., Schulz, B. L. & Fraser, J. A. A Genomic Safe Haven for
826 Mutant Complementation in *Cryptococcus neoformans*. *PLOS ONE* **10**, e0122916 (2015).

827 56. Tian, Y. *et al.* Quality and efficiency assessment of six extracellular vesicle isolation methods
828 by nano-flow cytometry. *Journal of Extracellular Vesicles* **9**, 1697028 (2020).

829 57. Moyrand, F., Lafontaine, I., Fontaine, T. & Janbon, G. UGE1 and UGE2 regulate the UDP-
830 glucose/UDP-galactose equilibrium in *Cryptococcus neoformans*. *Eukaryot Cell* **7**, 2069–2077
831 (2008).

832 58. Medical Mycology: Cellular and Molecular Techniques | Wiley. *Wiley.com*
833 <https://www.wiley.com/en-us/Medical+Mycology%3A+Cellular+and+Molecular+Techniques-p-9780470057407>.

835 59. Wallace, E. W. J. *et al.* Quantitative global studies reveal differential translational control by
836 start codon context across the fungal kingdom. *Nucleic Acids Res* **48**, 2312–2331 (2020).

837 60. Langmead, B. & Salzberg, S. L. Fast gapped-read alignment with Bowtie 2. *Nat Methods* **9**,
838 357–359 (2012).

839 61. Kim, D. *et al.* TopHat2: accurate alignment of transcriptomes in the presence of insertions,
840 deletions and gene fusions. *Genome Biol* **14**, R36 (2013).

841 62. Love, M. I., Huber, W. & Anders, S. Moderated estimation of fold change and dispersion for
842 RNA-seq data with DESeq2. *Genome Biol* **15**, 550 (2014).

843 63. Maufrais, C. *et al.* Population genomic analysis of *Cryptococcus* Brazilian isolates reveals an
844 African type subclade distribution. *G3 (Bethesda)* **11**, jkab107 (2021).

845 64. Li, H. Minimap2: pairwise alignment for nucleotide sequences. *Bioinformatics* **34**, 3094–3100
846 (2018).

847 65. Li, H. *et al.* The Sequence Alignment/Map format and SAMtools. *Bioinformatics* **25**, 2078–
848 2079 (2009).

849 66. Rosenberg, A. *et al.* Antifungal tolerance is a subpopulation effect distinct from resistance
850 and is associated with persistent candidemia. *Nat Commun* **9**, 2470 (2018).

851